3-1-1994

Search for Important Weak Interaction Nuclei in Presupernova Evolution

Maurice B. Aufderheide
E. Division and IGAPP - Lawrence Livermore National Laboratory

Ikko Fushiki
Ink Development Corporation

Stanford E. Woosley
Board of Studies in Astrophysics and Astronomy, University of California

Dieter H. Hartmann
Department of Physics and Astronomy, Clemson University, hdieter@clemson.edu

THE ASTROPHYSICAL JOURNAL SUPPLEMENT SERIES, 91:389–417, 1994 March

SEARCH FOR IMPORTANT WEAK INTERACTION NUCLEI IN PRESUPERNOVA EVOLUTION

MAURICE B. AUFDERHEIDE,[1] IKKO FUSHIKI,[2] STANFORD E. WOOSLEY,[3] AND DIETER H. HARTMANN[4]
Received 1993 March 29; accepted 1993 July 8

ABSTRACT

A search is made for the most important electron captures and beta-decays after core silicon burning in massive stars. A nuclear statistical equilibrium code is used to compute isotopic abundances. Electron capture and beta-decay rates are estimated for the 150 most abundant isotopes in a simplified fashion which generally includes the strongest transitions. These estimates are made for nuclei in the *fp*-shell and use techniques similar to Fuller, Fowler, & Newman (1982a), and are compared to them. The general behavior of $\dot{Y}_e$ is examined. These methods are then used to follow a typical stellar trajectory, seeking the most important weak interactions during the formation of the iron core. Ranked lists of nuclei are given, to prioritize more detailed studies on individual nuclei. Beta-decays are found to be an important modification to the evolution below $Y_e \approx 0.46$ as the core approaches a state of dynamic equilibrium between electron captures and beta-decays.

Subject headings: nuclear reactions, nucleosynthesis, abundances — stars: interiors — supernovae: general

1. INTRODUCTION

For many years it has been recognized that weak interactions, especially nuclear beta-decay and electron capture, are important during the late stages of stellar evolution. Hansen (1966, 1968), Mazurek (1973), and Mazurek, Truran, & Cameron (1974) computed such rates for a large array of nuclei using the best physics of the time. The gross theory of beta-decay (Takahashi & Yamada 1969; Koyama, Takahashi, & Yamada 1970; Takahashi 1971; Takahashi, Yamada, & Kondoh 1973) was used (Egawa, Yokoi, & Yamada 1975; Yokoi & Yamada 1976; Takahashi, El Eid, & Hillebrandt 1979) to calculate weak rates for many nuclei. Bethe et al. (1979) suggested that the newly discovered Gamow-Teller (GT) resonance could drastically increase electron capture rates and could affect the formation of the iron core in Type II supernova progenitors and the final collapse of the core. Fuller, Fowler, & Newman (1980, 1982a, b, 1985, hereafter FFN) used a simple shell model to compute the location and strength of such resonances for 226 nuclei with mass numbers 21 to 60. The inclusion of their rates in stellar evolution codes significantly affected the evolution of presupernova stars (Weaver, Woosley, & Fuller 1985) by causing a greater reduction in the electron fraction throughout the core.

Recently it has become clear that more work needs to be done on these rates. Aufderheide et al. (1990) emphasized that calculations of presupernova evolution generate cores that are so neutron-rich (Y_e, the electron fraction, reaches 0.42 and lower) that nuclei more massive than $A = 60$ must be considered, thus requiring an extension of the FFN rate tables. Kar, Sarkar, & Ray (1991) have begun work on β-decay nuclei with $A > 60$. It has been found (Aufderheide 1991; Aufderheide et al. 1993a,b) that the approach of FFN is not always reliable in its estimates of the location of GT strength when compared with the recent measurements (Vetterli et al. 1989; Alford et al. 1992) of GT strength by (n, p) experiments. Such circumstances call for a new evaluation of these rates for more nuclei than were considered by FFN.

In performing such a large tabulation, it is useful to start with the most important nuclei and proceed to less important ones as time and resources permit. Unfortunately, the nuclei which cause the largest changes in Y_e are neither the most abundant ones nor the ones with the strongest rates, but a combination of the two. In fact, the most abundant nuclei tend to have small rates (because they are more stable) and the most reactive nuclei tend to be present in small quantities. Thus one cannot simply use abundances or weak rates separately to determine the most important nuclei but must fold these sets of information together. Epstein & Arnett (1975) made such a study, but their work was limited by several factors. First, they used the rates of Hansen (1966, 1968) and Mazurek et al. (1974; Mazurek 1973), which do not include the GT resonances which are now known to be an important part of the rates for astrophysically relevant conditions. Second, their study was limited to values of Y_e between 0.45 and 0.50. Third, and less importantly, they used zero temperature partition functions in the calculation of their abundances, which compromises the abundance determination. An update of their study would thus be extremely useful for updating weak rates.

Unfortunately, there has been no systematic tabulation of rates for nuclei with $A > 60$, so there is no easy way to do the study. In this paper, we develop a fast and reasonably accurate approximation for electron capture and beta-decay rates which includes the most important physics. We then fold these rates into a set of abundances obtained assuming nuclear statistical equilibrium (NSE). From this we are able to predict, in an approximate way, which nuclei should be studied first to give an accurate representation of the total rate of change of Y_e for a given temperature (T), density (ρ), and Y_e. We examine the conditions typical of a presupernova core and provide a

[1] E Division and IGPP, L-413, Lawrence Livermore National Laboratory, Livermore, CA 94550.
[2] Ink Development Corporation, 1300 South El Camino Real, Suite 201, San Mateo, CA 94402.
[3] Board of Studies in Astrophysics and Astronomy, University of California, Santa Cruz, CA 95064.
[4] Department of Physics and Astronomy, Clemson University, Clemson, SC 29634.

ranked list of nuclei to be studied in greater detail in the future. Because we assume NSE, this work is only applicable after silicon burning is completed.

The paper is divided into six sections. The next two describe the approach used to compute abundances and weak interaction rates, while the last three sections discuss our results. Section 2 describes our treatment of NSE and the ingredients of such calculations: nuclear partition functions and nuclear mass laws. Section 3 describes our evaluation of electron capture and beta-decay rates and compares it to the FFN rates. In § 4 we explore the general behavior of the weak flows predicted by these rates for a range of temperatures, densities, and electron fraction. In § 5 we construct a typical stellar evolution trajectory in (ρ, T, Y_e) space and examine the weak flows along the trajectory. From this study we are able to compile a list of important nuclei. In the last section we describe the need for and nature of future work in this area.

2. NUCLEAR STATISTICAL EQUILIBRIUM

The rates that we wish to model become important after silicon burning is complete and the temperatures within the iron core are high enough that the strong and electromagnetic (but not weak) reactions are in equilibrium. In such a case, the nuclear Saha equation gives the abundance of each nuclear species as a function of ρ, T, Y_e, and the binding energy and partition function of each nucleus. Our treatment of NSE is similar to previous work (Clifford & Tayler 1965; Epstein & Arnett 1975; El Eid & Hillebrandt 1980; Hartmann, Woosley, & El Eid 1985), but we briefly repeat the formalism here for completeness.

Let the kth nucleus have charge and mass number Z and A, respectively, and $N = A - Z$. The binding energy is $Q_k = (Zm_{\rm H} + Nm_n - M_k)c^2$, where all masses are atomic. The mass fraction of the kth nucleus is given by X_k. The distribution of nuclei must conserve mass:

$$\sum_k X_k = 1 , \tag{1}$$

and charge:

$$\sum_k \frac{Z_k}{A_k} X_k = Y_e = \frac{(1-\eta)}{2} , \tag{2}$$

where η is the neutron excess. The abundance for nuclei other than neutrons and protons is given by

$$X_k = \frac{G(Z, A, T)}{2} \left(\frac{\rho N_{\rm A}}{2} \lambda^3 \right)^{A-1} \times A^{5/2} X_n^N X_p^Z \exp\left[Q_k / k_{\rm B} T \right] \tag{3}$$

where $G(Z, A, T)$ is the nuclear partition function for the kth nucleus, $N_{\rm A}$ is Avogadro's number, λ is the thermal wavelength: $\lambda = (h^2/2\pi m_{\rm H} k_{\rm B} T)^{1/2}$, and $k_{\rm B}$ is Boltzmann's constant. For a given set of thermodynamic conditions, X_n and X_p must be determined subject to equations (1) and (2) by iteration. After X_n and X_p are found, X_k can be calculated from equation (3).

Where available, we have used experimentally determined atomic masses (Wapstra & Audi 1985) to compute the binding energies. As the material becomes more neutron-rich, the distribution moves away from measured nuclei. In this case we have used the theoretical mass law of Comay, Kelson, & Zidon (1988). No effort has been made to smooth the transition from measured masses to theoretical estimates. In a future work we plan to investigate the sensitivity to theoretical mass laws.

An improvement which we have made with respect to the study of Epstein & Arnett (1975) is to use a true temperature dependent partition function, $G(Z, A, T)$, in equation (3) for each nucleus. Epstein & Arnett (1975) only used the ground state partition function $(2J_0 + 1)$. As temperature increases, $G(Z, A, T)$ becomes quite different from $(2J_0 + 1)$ and this affects the nuclear abundance substantially, especially for the more fragile nuclei of interest here, which have many low-lying excited states. This variation with temperature will be different with each nucleus, since it is a sensitive function of nuclear level density.

The nuclear partition function is given by

$$G(Z, A, T) = \sum_i (2J_i + 1) \exp\left[-\frac{E_i}{k_{\rm B} T} \right] \tag{4}$$

where J_i and E_i are the spin and energy of the ith state. If one knows the excited state distribution of a nucleus, this quantity is easily computed. Because many of the nuclei considered here are unstable and/or poorly studied at high excitation energy, it is not possible to have this information for each nucleus. Even for nuclei with some excited state information, one is still forced to use a theoretical representation of the level density for higher energies. We have used a simple parameterization in which the ground state spins have been taken from experiment where known and otherwise estimated using the shell model and Nordheim rules. The contribution from excited states was estimated using a level density formula, $\rho(E, J, \pi)$. The nuclear partition function was approximated by

$$G(Z, A, T) \approx (2J_0 + 1) + \int_0^\infty dE \int_{J,\pi} dJ d\pi (2J + 1) \times \rho(E, J, \pi) \exp\left[-E/k_{\rm B} T \right] . \tag{5}$$

The level density used is a backshifted Fermi gas formula (Holmes 1976; Woosley et al. 1975; Holmes et al. 1976) using the parameters of Thielemann, Arnould, & Truran (1986):

$$\rho(E, J, \pi) = \frac{1}{\sqrt{2\pi}\sigma} \frac{\sqrt{\pi}}{12 a^{1/4}} \times \frac{\exp\left[2\sqrt{a(E-\delta)} \right]}{(E-\delta)^{5/4}} f(E, J, \pi) , \tag{6}$$

$$f(E, J, \pi) = \frac{1}{2} \frac{(2J+1)}{2\sigma^2} \exp\left[-\frac{J(J+1)}{2\sigma^2} \right] ,$$

where a is the level density parameter, δ is the backshift (pairing correction), and σ is given by $(2m_u A R^2/5\hbar^2)^{1/2}[(E -$

$\delta)/a)]^{1/4}$. In the expression for σ, R is the radius and $m_u = 1/N_A$ is the atomic mass unit. The parameters δ and a are taken from Thielemann et al. (1986).

Examination of equation (5) reveals that the integrand has a minimum at approximately $E_{\min} \approx \delta + a(k_B T)^2$. At $E = \delta$, the level density becomes unphysically singular, which causes the increase in $\rho(E, J, \pi)$ below $E_{\min}$. For such low energies, the *Ansatz*

$$\rho_{\text{low}}(E) = \frac{1}{T} \exp\left[\frac{(E-\delta)}{T}\right] \tag{7}$$

is used for the level density, where T is determined by matching the slope of $\rho_{\text{low}}(E)$ and the backshifted Fermi gas at their intersection point. For more details about this approach, the reader is directed to pages 531–535 of Thielemann et al. (1986) or § 3.4.3 of Cowan, Thielemann, & Truran (1991).

In Figures 1*a*–1*d*, we provide a brief overview of the most abundant nuclei in an NSE distribution as a function of η for several values of temperature and density. Figure 1*a* uses the same conditions of Figure 2 of Hartmann et al. (1985, hereafter HWE), for comparison. The same nuclei are dominant in both treatments, but our peak abundances for ^{84}Se, ^{80}Zn, ^{79}Cu, and ^{78}Ni are somewhat less than in HWE. Our peak abundance for ^{68}Ni is somewhat higher than in HWE. The source of these differences is the use of different theoretical mass laws. All of these nuclei either have unknown masses, or neighboring nuclei have experimentally unknown masses for which a mass law is needed. HWE used the von Groote, Hilf, & Takahashi (1976) mass law and these masses are slightly different from those used here.

Figures 1*b*–1*d* show the top nuclei as a function of η for successively higher temperatures and densities. Density has been chosen to increase by an order of magnitude in each successive plot, and the temperature has been found by requiring these points to follow the stellar trajectory which will be discussed in § 5. It can be seen that, as temperature and density increase, the most abundant nuclei account for less of the total mass fraction within the gas (i.e., redistribution of mass occurs over larger numbers of nuclei, as expected on thermodynamic grounds). Also, it can be seen that new nuclei begin to appear in the plots. Increasing the density of the material tends to broaden out the distribution of nuclei. This tendency will be important for understanding how nuclei contribute to the weak flows.

3. WEAK INTERACTION RATES

3.1. *The General Problem*

As was said in the introduction, one of the difficulties in performing this study was the lack of electron capture and beta-decay rates for nuclei with mass greater than 60. Epstein & Arnett (1975) also faced this problem in their study, but their work was limited to $0.45 \leq Y_e \leq 0.5$, and the rate tables which they used appeared to have an adequate coverage of the nuclei which become abundant in this range. Indeed, the FFN rate tables also provide adequate coverage in this range, but we wish to study more neutron rich regimes.

Because of the current lack of reliable rate information for $A > 60$, it is necessary for us to develop estimates for these rates on heavy nuclei. Because we are considering hundreds of possible nuclei, it is not feasible to include detailed nuclear structure information for each nucleus and sum the contributions from individual transitions. Such a program would require a truly gigantic database which does not yet exist and the computation of roughly 30 phase space integrals for each nucleus in each direction (decay or capture). We thus seek approximations to the rates which allow us to include the most relevant physics in an economical way.

Before describing the approximations made in our approach, it is useful to consider the distribution of allowed GT and Fermi strength in these nuclei. Figure 2 provides a schematic description of the situation. We consider the nuclei (Z, A) and $(Z-1, A)$ and the allowed GT and Fermi transi-

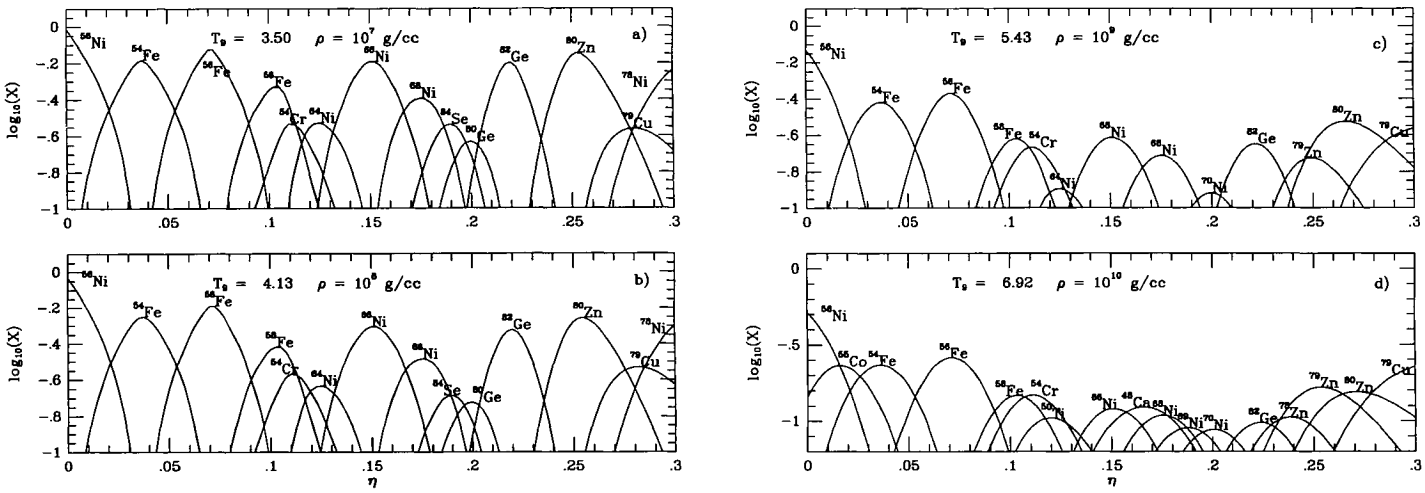

FIG. 1.—Mass fractions of the most abundant nuclei in NSE as a function of neutron excess, η, for increasing temperatures and densities. Note the dropping peak abundance with increasing temperature and density.

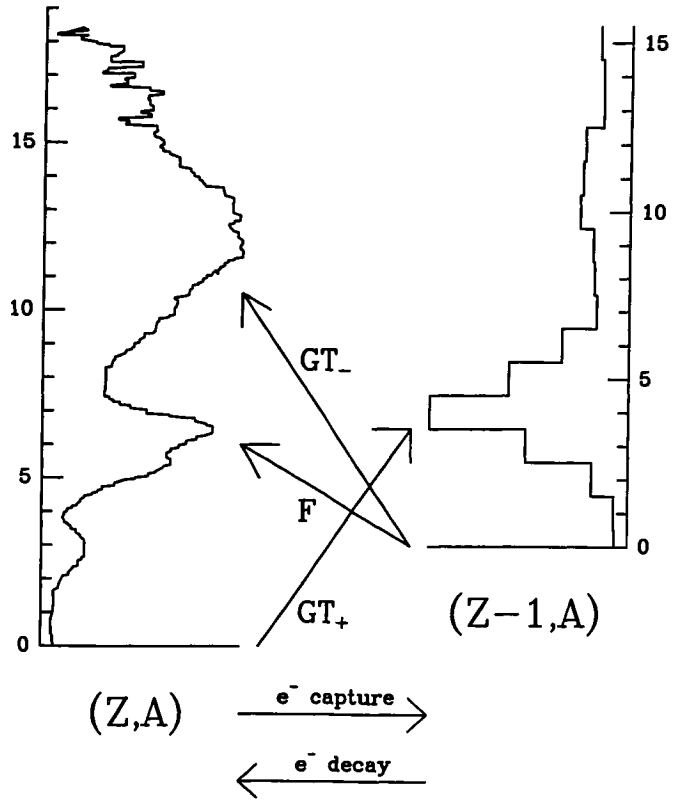

FIG. 2.—General distribution of GT strength in *fp* shell nuclei. Operating on the ground state of nucleus (Z, A) with the GT_+ operator produces the allowed GT strength function displayed in the $(Z-1, A)$ nucleus. This is the electron capture direction and is probed by intermediate energy (n, p) reactions. Similarly, operating on the ground state of nucleus $(Z-1, A)$ with the GT_- operator produces the allowed GT strength function displayed in the (Z, A) nucleus. This is the beta-decay direction and is probed by intermediate energy (p, n) reactions. Note that it is possible to thermally populate the resonant states in the parent nucleus which decay strongly to the daughter ground state. These strength functions exist for each parent and daughter excited state and must all be included in stellar rates.

tions from each to the other. Operating on the ground state of (Z, A) with the GT_+ operator will produce a distribution of allowed GT strength in $(Z-1, A)$ as is shown in the figure. This strength can be measured with intermediate energy (n, p) reactions and is concentrated in a resonance typically 1 to 10 MeV above the ground state of $(Z-1, A)$. Electron capture transitions proceed in this direction.

Operating on the ground state of $(Z-1, A)$ with the GT_- operator will produce a distribution of allowed GT strength in (Z, A) as is shown in the figure. This strength can be probed with intermediate energy (p, n) reactions and is concentrated in a giant resonance typically 5 to 15 MeV above the ground state of (Z, A). This giant resonance typically contains 3 times as much GT strength as does the resonance in the GT_+ direction. In addition to this strength, the allowed Fermi strength is concentrated in the isobaric analog state in the daughter nucleus, typically 5 to 15 MeV above the ground state. Beta-decay transitions proceed in this direction.

We have thus far only discussed transitions from the ground state of each nucleus. For each excited state, analogous resonances exist. In the astrophysical conditions of interest, the nuclei are in a thermal bath of $T \sim 3 \times 10^9$ K and higher, and their excited states are thermally populated. Thus, the GT strength in the daughter nucleus resulting from operating on each parent excited state with GT_+ (GT_-) must be known in order to calculate the electron capture (beta-decay) rate. The problem is even more complicated because one must also consider the thermal population of resonant states in the parent obtained by operating on any state in the daughter nucleus with GT_- (GT_+). These states, if thermally populated, will decay to the daughter state with great strength. These resonances will be called "back resonances" in this paper. For example, in computing the stellar electron capture rate for (Z, A), we need to know the locations of the resonances in $(Z-1, A)$ which result from operating on each state of (Z, A) with GT_+ and must weigh their contributions with a Boltzmann factor. We also need to compute the locations of the back resonances in (Z, A), which result from operating on the states of $(Z-1, A)$ with GT_- and must include these transitions with appropriate Boltzmann factors. A similar procedure must be followed in calculating beta-decay rates. In the case of electron capture rates, the back resonance due to the Fermi transition must also be included. Because the GT_- and Fermi resonances tend to be much higher above the ground state than the GT_+ resonance, back resonances become an important part of beta-decay at lower temperature than for electron capture.

3.2. *Electron Capture*

The calculations of FFN have shown that for densities above $\sim 10^7$ g cm^{-3}, electron capture transitions to the Gamow-Teller resonance are an important part of the rate. Such resonant captures happen only when the material has become dense enough that the electron chemical potential is large enough to enable the electrons to sample the resonance. Any reliable simulation of the rates under these conditions must include this strength, at least in an approximate fashion.

The electron capture rate for the kth nucleus (Z, A) can be written in the form

$$\lambda_k^{ec}(\rho, T, Y_e) = \ln 2 \sum_i \frac{(2J_i + 1) \exp[-E_i/k_B T]}{G(Z, A, T)} \times \sum_j \frac{\phi(\rho, T, Y_e, Q_{ij})}{ft_{ij}}, \quad (8)$$

where i denotes parent state, j denotes the daughter state, J_i and E_i are the spin and excitation energy of the ith parent state, G is the nuclear partition function, ϕ is the standard electron capture phase space integral defined below, Q_{ij} is the *nuclear* energy difference between states i and j, respectively, and ft_{ij} is the ft-value connecting states i and j. For the nuclei of interest here, the ft-value contains the GT matrix element for the transition and can be expressed as (Fuller et al. 1980)

$$\frac{1}{ft_{ij}} = \frac{|M_{ij}|^2}{10^{3.596}}, \quad (9)$$

where M_{ij} is the GT matrix element for the transition. The electron capture phase space integral can be written in the

form

$$\phi(\rho, T, Y_e, Q_{ij}) = \frac{c^3}{(m_e c^2)^5} \int_{\mathscr{L}}^{\infty} dp p^2 (Q_{ij} + E_e)^2 \times \frac{F(Z, E_e)}{1 + \exp[(E_e - \mu_e)/k_B T]}, \quad (10)$$

where p, E_e, and μ_e are the electron momentum, energy, and chemical potential, $F(Z, E_e)$ is the Fermi function discussed below, and $\mathscr{L} = (Q_{ij}^2 - m_e^2 c^4)^{1/2}$ for $Q_{ij} \leq -m_e c^2$ (0 otherwise). The Fermi function corrects the phase space integral for the Coulomb distortion of the electron wavefunction near the nucleus. It can be written as

$$F(Z, E_e) = \frac{|\psi_{\text{Coulomb}}|^2}{|\psi_{\text{free}}|^2} = 2(1+\gamma)\left(\frac{2 p_e R}{\hbar}\right)^{-2(1-\gamma)} e^{\pi\nu} \frac{|\Gamma(\gamma + i\nu)|^2}{|\Gamma(2\gamma+1)|^2}, \quad (11)$$

where $\nu = Z\alpha(E_e/\text{pc})$, $\gamma = [1 - (Z\alpha)^2]^{1/2}$, R is the nuclear radius, Γ is the gamma function, and α is the fine-structure constant. We do not use any limiting forms for the Fermi function, but use the Lanczos (1964) technique to evaluate the gamma functions. For the calculations in this paper, the phase space integrals have been computed numerically.

Because of the scope of this calculation, it is not feasible to explicitly perform the sums over parent and daughter states required by equation (8). We have broken the sum over j, daughter states, into two pieces and handled them separately. If we denote the sum of transitions from parent state i to all accessible daughter states as S_i, we make the following division:

$$\begin{aligned} S_i(\rho, T, Y_e) &\equiv \sum_j \frac{\phi(\rho, T, Y_e, Q_{ij})}{ft_{ij}} \\ &= \sum_{j \in \substack{\text{low} \\ \text{energy}}} \frac{\phi(\rho, T, Y_e, Q_{ij})}{ft_{ij}} + \sum_{j \in \text{GTR}} \frac{\phi(\rho, T, Y_e, Q_{ij})}{ft_{ij}} \\ &\approx \frac{\phi(\rho, T, Y_e, Q_{00})}{ft_{\text{eff}}} + \frac{\phi(\rho, T, Y_e, Q_{i\text{GTR}(i)})}{ft_{i \to \text{GTR}(i)}}, \end{aligned} \quad (12)$$

where ft_{eff} is an effective ft-value to represent the effects of transitions to low-energy daughter states, Q_{00} is the ground state to ground state nuclear Q-value, and the "$i \to \text{GTR}(i)$" subscript in the second term of equation (12) refers to transitions from the ith parent state to higher lying daughter states, dominated by the GT resonance corresponding to the ith parent state. Several approximations have been made. First, all of the transitions to low-lying daughter states have been put into the first term, which has been given an effective ft-value. Second, the transitions at high daughter energy are assumed to be dominated by the GT resonance. The last approximation is to place all of the GT resonance strength from the ith parent state into a single transition to a state with energy $E_{\text{GTR}(i)}$ above the daughter ground state. This approximate treatment is similar to the FFN approach. The transitions to low-lying states which FFN include in their rates in some form have been lumped into the first term of equation (12). The transition to the GT resonance, embodied in the second term of equation (12), is included in the rate exactly as FFN did it.

The second FFN paper (Fuller et al. 1982a) describes in detail how the location and strength in these resonances can be estimated. It is standard to assume that the location of the GT resonance moves upward in the daughter nucleus by the same amount as the energy separation between the ith parent state and the parent ground state:

$$E_{\text{GTR}(i)} = E_{\text{GTR}(0)} + E_i . \quad (13)$$

This assumption (known as the Brink hypothesis in electromagnetic transitions; Holmes 1976) was made by FFN and its reasonableness has been argued for the example of ^{54}Fe by Aufderheide (1991). Aufderheide et al. (1993a) demonstrate with shell model calculations that this relation is accurate for $^{59}\text{Co}(e^-, \nu_e)^{59}\text{Fe}$ to within 100 keV for the lowest several states of ^{59}Co. From this assumption and equation (13) follows

$$\begin{aligned} Q_{i\,\text{GTR}(i)} &= Q_{00} + E_i - E_{\text{GTR}(i)} \\ &= Q_{00} - E_{\text{GTR}(0)}, \end{aligned} \quad (14)$$

where the dependence on parent states has canceled. It is also assumed by FFN and here that $ft_{i \to \text{GTR}(i)} = ft_{0 \to \text{GTR}(0)}$ is the same for all parent states. The shell model calculations mentioned above verify this assumption to within roughly 20%.

As a result of these assumptions, the second term in equation (12) loses its dependence on parent states as did the first term. The electron capture rate, equation (8), thus takes the final form

$$\lambda_k^{\text{ec}}(\rho, T, Y_e) \approx \ln 2 \left\{ \frac{\phi(\rho, T, Y_e, Q_{00})}{ft_{\text{eff}}} + \frac{\phi(\rho, T, Y_e, Q_{00} - E_{\text{GTR}(0)})}{ft_{0 \to \text{GTR}(0)}} \right\}. \quad (15)$$

The effective ft-value was chosen to fit the FFN rates as well as possible in the range $0.45 \leq Y_e \leq 0.50$. It was found that $ft_{\text{eff}} = 6.06 \times 10^4$ provided the best fit.

The values for $ft_{0 \to \text{GTR}(0)}$ and $E_{\text{GTR}(0)}$ were determined using the methods described in the second FFN paper (1982a). We provide a brief description here of the method using $^{58}\text{Co}(e^-, \nu_e)^{58}\text{Fe}$ as an example. The first step is to build a simple shell model of the parent nucleus, neglecting configuration mixing and excitations. Figure 3 shows how ^{58}Co is treated. For electron capture, a proton is turned into a neutron by a GT transition. Fermi transitions are blocked. All seven fp protons are in the $1f_{7/2}$ orbital and thus the only allowed GT transitions are

to the $1f_{7/2}$ and $1f_{5/2}$ neutron orbitals. The former orbital is blocked by neutrons. Thus the GT resonant state in the daughter nucleus is as shown in Figure 3; the $1f_{7/2}$ proton has become a $1f_{5/2}$ neutron. The energy difference between the resonant state and the ground state, $E_{\mathrm{GTR}(0)}$, is estimated using the formula

$$E_{\mathrm{GTR}(0)} = \Delta E_{\mathrm{SPE},n} + \Delta E_{\mathrm{ph}} + \Delta E_{\mathrm{pair}} , \qquad (16)$$

where $\Delta E_{\mathrm{SPE},n}$ is the energy difference between the orbitals which the new neutron occupies in the GT resonance and the ground state (estimated by using single particle energies), ΔE_{ph} is the particle-hole repulsion energy which must be supplied to pull the neutron out of the daughter ground state, ΔE_{pair} is the cost to break a neutron pair if there is an even number of neutrons in the daughter nucleus. In the case of ^{58}Co, $E_{\mathrm{GTR}(0)}$ becomes

$$\begin{aligned} E_{\mathrm{GTR}(0)} &= (\epsilon_{1f_{5/2}} - \epsilon_{2p_{3/2}})|_n + \Delta E_{\mathrm{ph}} + \Delta E_{\mathrm{pair}} \\ &= \left[\frac{119.4 - 112.6}{58^{1/3}} + 2 + \frac{12}{\sqrt{58}}\right] \mathrm{MeV} \\ &= 5.332 \text{ MeV} . \end{aligned} \qquad (17)$$

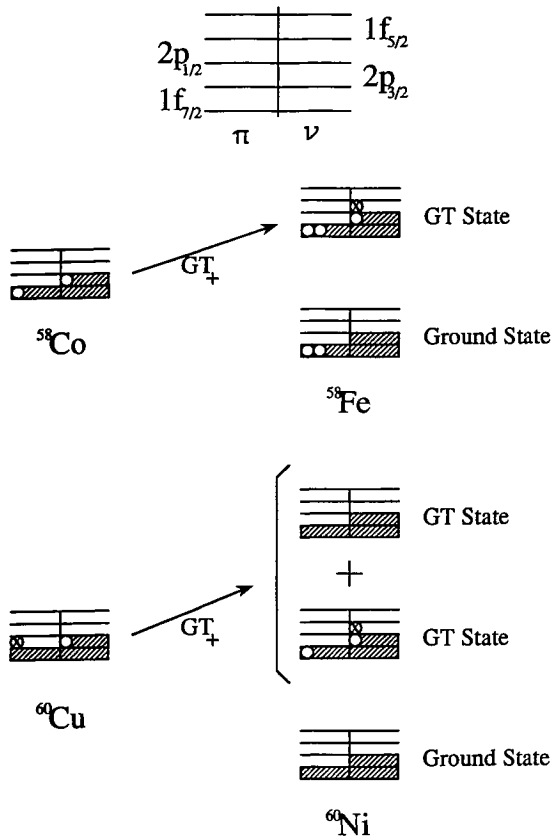

FIG. 3.—Simple shell models for estimate of GT resonant transitions from ^{58}Co and ^{60}Cu. At the top is an explanation of the shell model diagram used to characterize the nuclei. "π" refers to protons, while "ν" refers to neutrons. The case of ^{58}Co is listed in the middle and the case of ^{60}Cu is at the bottom. For each nucleus, the daughter ground state and all possible GT resonant configurations which can be produced by operating on the parent nucleus with GT_+ are listed.

TABLE 1

SEEGER SINGLE PARTICLE ENERGIES FOR THE *fp* SHELL

Orbital	Single Particle Energy (MeV × $A^{1/3}$)
$2p_{1/2}$	123.2
$1f_{5/2}$	119.4
$2p_{3/2}$	112.6
$1f_{7/2}$	94.7

Following FFN, we have used the Seeger single particle energies, as listed in Hillman & Grover (1969). Table 1 lists the *fp* shell energies.

The amount of strength in the GT transition is also estimated using simple shell model arguments. The resonant GT matrix element is calculated using

$$|M_{\mathrm{GTR}(0)}|^2 = \frac{n_i^p n_f^h}{2j_f + 1} |M_{\mathrm{GT}}^{\mathrm{sp}}|_{if}^2 , \qquad (18)$$

where n_p^i is the number of proton particles in the initial orbital, n_f^h is the number of neutron holes in the final (daughter) orbital, and $|M_{\mathrm{GT}}^{\mathrm{sp}}|_{if}^2$ is the square of the single particle GT matrix element from the initial orbital to the final orbital. Table 2 gives these matrix elements.

It is well-known that not all of the GT strength appears at the relatively low energies predicted by shell model calculations. This phenomenon has been called "quenching" (Gaarde, Larson, & Rapaport 1982; Goodman & Bloom 1982). The GT resonances included in the published FFN tables (Fuller et al. 1982b) are not quenched because the phenomenon of quenching was just being discovered at the time. In their last paper (Fuller et al. 1985), FFN note this fact and include a phenomenological quenching factor in their effective log ft factors. When their rate is dominated by transitions involving the GT resonance, the rates should be reduced by a factor of 2 (Fuller 1992). The difficulty is in knowing what fraction of the FFN rate is due to the GT resonance and thus which part of the rate to quench. In our effective rates, we quench the resonant GT matrix element by a factor of 2 in all cases, except when we wish to compare with the FFN rates.

In cases where the protons can be transformed into both allowed neutron orbitals, we compute the strength for both transitions and put all of the strength into the "spin flip chan-

TABLE 2

VALUE OF THE SINGLE PARTICLE GT MATRIX ELEMENT, $|M_{\mathrm{GT}}^{\mathrm{sp}}|_{if}^2$

	j_f	
j_i	$l + 1/2$	$l - 1/2$
$l + 1/2$	$\frac{l + 3/2}{l + 1/2}$	$\frac{2l}{l + 1/2}$
$l - 1/2$	$\frac{2l + 2}{l + 1/2}$	$\frac{l - 1/2}{l + 1/2}$

nel" (the transition which changes j), in order to follow FFN conventions (Fuller 1992). Applying these rules to ^{58}Co, we obtain

$$|M_{\mathrm{GTR}(0)}|^2 = \frac{7 \times 6}{6} \frac{12}{7} \frac{1}{2} = 6 \qquad (19)$$

where we have quenched the GT strength.

Because we consider nuclei more massive than $A = 60$, we sometimes encounter cases where the parent nucleus has protons in more than one *fp* shell orbital. An example of this case, ^{60}Cu, is shown in Figure 3. This nucleus can have resonant transitions from either $1f_{7/2}$ or $2p_{3/2}$ proton orbitals. In such cases, the electron capture rate has several terms like the second term in equation (15), including the GT resonant transition from each parent single particle level separately.

For the calculations described in this paper, we have limited our treatment of resonances to the *fp* shell. For nuclei which are above or below this shell, we only compute the first term of equation (15). This is not a concern for the light nuclei, since they will not be abundant under the conditions we consider. But as the material becomes more dense and more neutron rich, the most abundant nuclei are increasingly massive. The neglect of GT resonances for these nuclei is probably not adequate, but we are uncertain about how to properly treat resonances in such nuclei. Because these nuclei involve transitions across oscillator shells, very little theoretical work has been done on them. Except for ^{208}Pb and ^{90}Zr, there has not yet been much (n, p) work either. Because of this ignorance, we have not tried to do better for this paper. At least the inclusion of an effective *ft*-value allows these nuclei to be included in a crude way in our study. We limit this study to cases where such nuclei do not dominate the changes in Y_e.

For this study, we have not included in our electron capture rates all of the GT resonance strength that was included by FFN. We do not include thermal population of back resonances in our electron capture rates. Since this study is only concerned with presupernova evolution, and not core collapse, it is not necessary to include such high temperature phenomena. Our electron capture rates are thus only accurate up to roughly $T_9 \approx 6.5$. We hope in the future to include such resonances.

It is clear from the above discussion that we have used the FFN approach to computing electron capture rates for *fp* shell nuclei. In particular, we have used their approach to computing the location and strength in the GT resonances. Recent work (Aufderheide 1991; Aufderheide et al. 1993a,b) has questioned the accuracy of these methods. We have used the FFN methods for two reasons. First, the FFN approach is the only method in the literature which allows a quick, systematic estimate of GT resonances. Second, although the recent work has shown inadequacies in the FFN approach for several nuclei, it is not far enough along to tell how to improve the situation.

As can be seen in equation (15) our estimate of the electron capture rate is a rather drastic approximation. We do not explicitly include all of the low-lying transitions. This weakness can compromise the rate before it becomes dominated by the GT resonance. In § 3.4, these effective rates are compared with the FFN rates. Several cases will be seen where important nuclei, not yet dominated by GT resonances, are poorly estimated by the effective rate.

3.3. *Beta-Decay*

Beta-decay rates, although dominated by GT transitions (just as electron capture rates), have quite different behavior because of different phase space and the form of the GT resonances in this direction. In beta-decay, because electrons are being emitted, the phase space integral is only able to sample a small, low-energy, portion of the daughter spectrum. As a result, beta-decay rates tend to be more difficult to estimate since the parent to low-lying daughter state transitions are weak and highly variable. However, in this case the back resonances are much lower than in the electron capture case and can dominate the rate even at the relatively low temperatures encountered in presupernova evolution. These resonances must be included in the rate.

The beta-decay rate for the kth nucleus (Z, A) can be written

$$\lambda_k^{\mathrm{bd}}(\rho, T, Y_e) = \ln 2 \sum_i \frac{(2J_i + 1) \exp[-E_i/k_{\mathrm{B}}T]}{G(Z, A, T)} \times \sum_j \frac{\xi(\rho, T, Y_e, Q_{ij})}{ft_{ij}}, \qquad (20)$$

where all quantities are as defined in § 3.2 and $\xi(\rho, T, Y_e, Q_{ij})$ is the beta-decay phase space integral. This integral has the form

$$\xi(\rho, T, Y_e, Q_{ij}) = \frac{c^3}{(m_e c^2)} \int_0^{\sqrt{Q_{ij}^2 - m_e^2 c^4}} dp p^2 (Q_{ij} - E_e)^2 \times \frac{F(Z+1, E_e)}{1 + \exp[(\mu_e - E_e)/k_{\mathrm{B}}T]} \qquad (21)$$

and all quantities are as defined above. Because of the finite range of this integral, the sum over the daughter states, j, in equation (20) is limited to those states for which Q_{ij} is greater than $m_e c^2$.

Because of the behavior of $\xi(\rho, T, Y_e, Q_{ij})$, and the location of GT strength as described above, we break up the sums in equation (20) differently than in the electron capture case. In this case we break up the sum on parent states into a piece containing parent states close to the ground state and a piece containing parent states dominated by the back resonances,

$$\begin{aligned}\lambda_k^{\mathrm{bd}}(\rho, T, Y_e) &= \ln 2 \sum_{i \in \substack{\mathrm{low} \\ \mathrm{energy}}} \frac{(2J_i + 1) \exp[-E_i/k_{\mathrm{B}}T]}{G(Z, A, T)} \times \sum_j \frac{\xi(\rho, T, Y_e, Q_{ij})}{ft_{ij}} \\ &\quad + \ln 2 \sum_{i \in \substack{\mathrm{high} \\ \mathrm{energy}}} \frac{(2J_i + 1) \exp[-E_i/k_{\mathrm{B}}T]}{G(Z, A, T)} \times \sum_j \frac{\xi(\rho, T, Y_e, Q_{ij})}{ft_{ij}} \\ &\approx \ln 2 \frac{(2J_0 + 1)}{G(Z, A, T)} \exp[-E_{\mathrm{peak}}/k_{\mathrm{B}}T]\end{aligned}$$

$$\times \frac{\xi(\rho, T, Y_e, E_{\rm peak} + Q_{00})}{ft_{\rm eff}}$$

$$+ \ln 2 \sum_{i \in \substack{\text{high} \\ \text{energy}}} \frac{(2J_i + 1) \exp[-E_i/k_{\rm B}T]}{G(Z, A, T)} \times \sum_j \frac{\xi(\rho, T, Y_e, Q_{ij})}{ft_{ij}} . \quad (22)$$

We have approximated the transitions from low-lying parent states to all accessible daughter states by a single transition from a state $E_{\rm peak}$ above the ground state of the parent to the daughter ground state with an effective log ft-value of 5. How $E_{\rm peak}$ is determined and the treatment of the higher lying parent states will be discussed below.

The transitions from parent states of low excitation energy to all daughter states tend to be weak (log $ft \geq 5$ in the iron region) and the phase space integral favors the transitions with the largest Q-values. These facts explain our choice of log $ft_{\rm eff}$ and using only $j = 0$ in the sum over daughter states. The low-lying state in the parent which will make the largest overall contribution to the beta-decay rate is the one for which $\exp[-E_i/k_{\rm B}T] \times \xi(\rho, T, Y_e, E_i + Q_{00})$ is a maximum. If Q_{00} is negative and/or if μ_e is not much less than Q_{00}, this function will be peaked somewhere above the ground state of the parent. In our study, we have assumed that there will always be a state with a typical log ft near the peak of this function, defined as $E_{\rm peak}$ here. It is thus necessary to compute $E_{\rm peak}$.

The energy at which this function peaks is found by seeking the function's extremum:

$$\frac{\partial}{\partial E} \{\exp[-E/k_{\rm B}T] \times \xi(\rho, T, Y_e, E + Q_{00})\} = 0 , \quad (23)$$

and solving for $E = E_{\rm peak}$. Because of the complexity of $\xi(\rho, T, Y_e, E)$, it is not possible to obtain $E_{\rm peak}$ analytically. However, we have have obtained an excellent fit to $E_{\rm peak}$ as a function of T, μ_e, and Q_{00}. If we approximate ξ in equation (23) by $(E + Q_{00} - \mu_e)^5$, we can obtain an estimate of $E_{\rm peak}$:

$$E^0_{\rm peak} = 5T - Q_{00} + \mu_e , \quad (24)$$

where T is in MeV. This first-order estimate can be off by several MeV for some choices of the parameters.

The difference between $E_{\rm peak}$ and $E^0_{\rm peak}$, $\delta(T, \mu_e)$, is well fit by

$$\delta(T, \mu_e) = -0.6604 + 0.9429T - 0.02119\mu_e - 0.9432T\mu_e - 0.0009524\mu_e^2 + 0.06224T\mu_e^2 \quad (25)$$

over a temperature ranging from roughly 0.3 MeV to 0.8 MeV and electron chemical potentials ranging from 0.5 MeV up to at least 8 MeV. Approximating $E_{\rm peak}$ by

$$E_{\rm peak} \approx E^0_{\rm peak} + \delta(T, \mu_e) \quad (26)$$

is now accurate to within roughly 100 keV within this range.

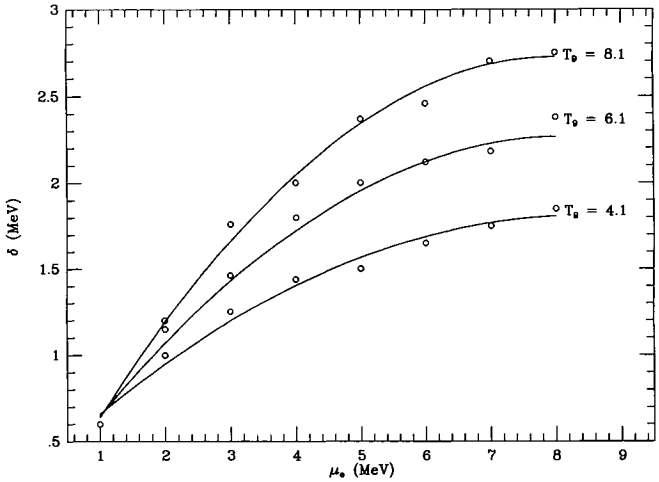

FIG. 4.—Comparison of the actual δ (the difference between $E_{\rm peak}$ and eq. [24]) (*circles*) with its fit (*solid curves*), eq. (25), as a function of electron chemical potential. Q_{00} is chosen to be −2 MeV here. Each curve and set of points refers to a different temperature.

Figure 4 demonstrates the quality of the fit. For values of T and μ_e outside the range listed above, the decay rates tend to be so weak as to be unimportant. If $E_{\rm peak}$ is negative, the ground state to ground state transition is computed. This approach can overestimate the contribution from low-energy parent states because it assumes that there will always be a parent state at $E_{\rm peak}$ which can make an allowed transition with log $ft = 5$ to the daughter ground state. However, this approach becomes an underestimate at high temperatures, as more parent states are thermally populated.

The higher lying parent states are assumed to be dominated by the back resonances. Let the beta-decay parent nucleus be (Z, A) and the daughter nucleus be denoted by $(Z + 1, A)$. To every state in $(Z + 1, A)$, there will correspond a back resonance in (Z, A) whose location in the parent can be estimated as was done in § 3.2. Let the excitation energy of this back resonance in the parent be denoted by $E_{{\rm BGTR}(j)}$, where the j refers to the state in the daughter to which it corresponds. Using the shifting assumption discussed above, the Q value for decays of these resonances becomes

$$Q_j = Q_{00} + E_{{\rm BGTR}(j)} - E_j = Q_{00} + {}_{\rm BGTR(0)} , \quad (27)$$

and the dependence on daughter excitation energy cancels. This is the analogous result to equation (14).

There will be some states in the region of the back resonance which will not be resonant. In our approximation, they are neglected because they are 10 to 100 times weaker than the back resonance strength. We will also neglect decays from all high-lying parent states to daughter states above the daughter ground state. Again, the resonant decay to the daughter ground state dominates, because of both matrix element and phase space considerations. Thus, for a daughter state j, the only term in the sum on high-energy parent states which survives in this approximation will be the state $i = \theta(j)$, which refers to the

back resonance in the parent. The beta-decay rate becomes

$$\lambda_k^{\rm bd}(\rho, T, Y_e) \approx \ln 2 \frac{(2J_0+1)}{G(Z,A,T)} \exp\left[-E_{\rm peak}/k_{\rm B}T\right] \times \frac{\xi(\rho, T, Y_e, E_{\rm peak}+Q_{00})}{ft_{\rm eff}} + \ln 2 \sum_j \frac{(2J_{\theta(j)}+1)\exp\left[-E_{\theta(j)}/k_{\rm B}T\right]}{G(Z,A,T)} \times \frac{\xi(\rho, T, Y_e, Q_j)}{ft_{{\rm BGTR}(j)\to j}}, \quad (28)$$

where the sum is over all daughter states in $(Z+1, A)$ and Q_j is as given above. The methods of § 3.2 allow us to compute $ft_{j\to{\rm GTR}(j)}$. We use detailed balance to obtain $ft_{{\rm BGTR}(j)\to j}$:

$$\frac{(2J_j^Z+1)}{ft_{{\rm BGTR}(j)\to j}} = \frac{(2J_j^{Z+1}+1)}{ft_{j\to{\rm GTR}(j)}}, \quad (29)$$

where the superscript on the J-values allows us to keep track of which nucleus we mean. If we approximate $ft_{j\to{\rm GTR}(j)}$ by $ft_{0\to{\rm GTR}(0)}$, as was done for electron capture, and use detailed balance, the beta-decay rate becomes

$$\lambda_k^{\rm bd}(\rho, T, Y_e) \approx \ln 2 \frac{(2J_0+1)}{G(Z,A,T)} \exp\left[-E_{\rm peak}/k_{\rm B}T\right] \times \frac{\xi(\rho, T, Y_e, E_{\rm peak}+Q_{00})}{ft_{\rm eff}} + \ln 2 \sum_j \frac{(2J_j^{Z+1}+1)\exp\left[-E_{\theta(j)}/k_{\rm B}T\right]}{G(Z,A,T)} \times \frac{\xi(\rho, T, Y_e, Q_j)}{ft_{0\to{\rm BGTR}(0)}}, \quad (30)$$

$$\approx \ln 2 \frac{(2J_0+1)}{G(Z,A,T)} \exp\left[-E_{\rm peak}/k_{\rm B}T\right] \times \frac{\xi(\rho, T, Y_e, E_{\rm peak}+Q_{00})}{ft_{\rm eff}} + \ln 2 \exp\left[-\frac{E_{\rm BGTR(0)}}{k_{\rm B}T}\right] \frac{G(Z+1,A,T)}{G(Z,A,T)} \times \frac{\xi(\rho, T, Y_e, Q_{00}+E_{\rm BGTR(0)})}{ft_{0\to{\rm BGTR}(0)}}, \quad (31)$$

where we have used the shifting assumption to express $E_{\theta(j)}$ as $E_{\rm BGTR(0)}+E_j$ and have used the definition of the Q-value given in equation (27). Although the resonant piece of the decay rate is damped by the exponential, $E_{\rm BGTR(0)}$ is not so large that it overcomes the strength of the matrix element and the large phase space integral. Thus this piece tends to dominate the decay rate, just as the resonant piece dominated the electron capture rate. In the next section we discuss the results generated from our approach.

3.4. *Comparison of Effective Rates With FFN Rates*

As was noted in the introduction, knowledge of neither abundances nor rates by themselves is sufficient for determining the most important electron capture or beta-decay nuclei for given values of ρ, T, and Y_e. What really matters for stellar evolution is $\dot{Y}_e$, the rate of change of Y_e caused by each nucleus. The rate of change of Y_e due to electron captures (beta decays) on the kth nucleus is given by

$$\dot{Y}_e^{\rm ec(bd)}(k) = -(+)\frac{X_k}{A_k}\lambda_k^{\rm ec(bd)}. \quad (32)$$

The quantity $\dot{Y}_e$ is negative for electron capture, while it is positive for beta decay. Whenever nuclei are ranked or compared, we will be using $\dot{Y}_e$ as the criterion for determining relative importance. For all of the lists of nuclei which will be discussed in this paper, we have computed weak interaction rates for the 150 most abundant nuclei. We have determined by examining the effects of less abundant nuclei that the largest contributors to $\dot{Y}_e$ are always within this set of nuclei, for densities below roughly 10^{11} g cm^{-3}. As density increases, the distribution of nuclei becomes much broader, i.e., more nuclei are present in the abundance peak. This trend was seen in Figures 1*a*–1*d*. Under these conditions, the total $\dot{Y}_e$ is a sum of small contributions from many nuclei. No single nucleus is dominant. As the density approaches 10^{11} g cm^{-3}, more than 150 nuclei may be necessary to accurately compute the total changes in Y_e. This problem is not too worrisome for this study, since the scope is limited to precollapse evolution.

Four ρ, T_9, and Y_e points have been chosen for making comparisons of the effective rates with the original FFN rates. Table 3 provides a key to these comparisons. The electron capture rates and beta decay rates are compared in the eight tables which follow Table 3. Tables 4–7 compare the electron capture rates at these four points, while Tables 8–11 compare the beta-decay rates. These points were chosen because they roughly characterize the path that the central regions of massive stars follow after core silicon burning. We will discuss this path in greater detail in § 5. The effective rates which we list here were computed with unquenched GT matrix elements, to facilitate comparison with the unquenched FFN rates.

We begin by comparing the total rate of change in Y_e due to electron capture and beta-decay for all four points. In the case of electron capture, it can be seen that the total $\dot{Y}_e$ computed with the effective rates and with the FFN rates are within 30% of one another at the lower densities. As density increases, the

TABLE 3

SUMMARY OF CONDITIONS USED FOR COMPARISON OF EFFECTIVE AND FFN RATES

ρ (g cm^{-3})	T_9	Y_e	Capture Table	Decay Table
5.86 (7)	3.40	0.47	4	8
1.45 (8)	3.80	0.45	5	9
1.06 (9)	4.93	0.43	6	10
4.01 (10)	7.33	0.41	7	11

TABLE 4

LIST OF NUCLEI
(ELECTRON CAPTURE: ρ = 5.86E+07, T_9 = 3.40E+00, Y_e = 0.47000)

^AZ	X_k	λ_k^{ec} (s^{-1})	$\lvert \dot{Y}_e^{ec}(k) \rvert$ (s^{-1})	λ_k^{ec} FFN (s^{-1})	Ratio	$\mathcal{F}$	Fraction GT
^{57}Co	3.55E−02	3.50E−03	2.18E−06	1.89E−03	1.85E+00	3	3.75E−02
^{55}Fe	5.20E−02	1.61E−03	1.52E−06	1.57E−03	1.03E+00	1	7.24E−05
^{55}Co	5.35E−04	1.41E−01	1.37E−06	1.36E−01	1.04E+00	2	8.69E−01
^{54}Fe	2.11E−01	3.11E−04	1.21E−06	2.95E−04	1.05E+00	4	3.07E−03
^{56}Co	5.56E−04	7.40E−02	7.35E−07	6.91E−02	1.07E+00	5	6.09E−01
^{53}Mn	1.30E−02	2.48E−03	6.09E−07	1.30E−03	1.91E+00	8	1.53E−02
^{58}Ni	5.44E−02	6.36E−04	5.97E−07	3.72E−04	1.71E+00	7	6.36E−03
^{59}Ni	5.13E−03	4.37E−03	3.80E−07	4.31E−03	1.01E+00	6	6.85E−04
^{61}Cu	5.00E−05	3.93E−01	3.22E−07	...	...	...	9.73E−01
^{57}Ni	1.71E−04	1.94E−02	5.84E−08	9.93E−03	1.96E+00	9	9.19E−02
^{58}Co	1.31E−04	1.04E−02	2.35E−08	3.68E−03	2.84E+00	14	9.49E−03
^{54}Mn	2.16E−04	5.13E−03	2.05E−08	1.41E−03	3.64E+00	16	5.83E−04
^{51}Cr	3.57E−04	2.81E−03	1.97E−08	1.31E−03	2.14E+00	13	2.23E−11
^{62}Cu	7.23E−07	1.59E+00	1.85E−08	...	...	...	9.85E−01
^{52}Mn	2.97E−05	2.85E−02	1.62E−08	7.24E−03	3.93E+00	17	1.05E−06
^{53}Fe	2.52E−05	2.04E−02	9.70E−09	3.91E−02	5.21E−01	10	1.03E−07
^{56}Ni	2.72E−05	1.60E−02	7.76E−09	1.30E−02	1.23E+00	15	3.96E−01
^{59}Cu	2.69E−07	1.01E+00	4.62E−09	1.37E−01	7.43E+00	20	9.67E−01
^{60}Cu	3.07E−07	8.39E−01	4.30E−09	1.20E−01	7.01E+00	21	9.40E−01
^{60}Ni	8.90E−02	1.49E−06	2.21E−09	9.17E−06	1.63E−01	12	3.26E−01

$\dot{Y}_e^{tot}$ = −9.12E−06 s^{-1}, $\dot{Y}_e^{tot}$(FFN) = −6.98E−06 s^{-1}

NOTES.—List of 20 nuclei with the largest $\lvert \dot{Y}_e \rvert$'s, sorted in order of $\lvert \dot{Y}_e \rvert$. In computing $\lvert \dot{Y}_e \rvert$ for each nucleus, the effective rates are used. An entry characterized by "..." means that there is no corresponding FFN rate. The "Ratio" column computes $\lambda_{eff}/\lambda_{FFN}$ for each nucleus. The "$\mathcal{F}$" column lists in what order these nuclei would have been ranked if the FFN rates had been used in forming $\lvert \dot{Y}_e \rvert$. The last column lists what fraction of the effective rate is given by transitions involving the GT resonance.

TABLE 5

LIST OF NUCLEI
(ELECTRON CAPTURE: ρ = 1.45E+08, T_9 = 3.80E+00, Y_e = 0.45000)

^AZ	X_k	λ_k^{ec} (s^{-1})	$\lvert \dot{Y}_e^{ec}(k) \rvert$ (s^{-1})	λ_k^{ec} FFN (s^{-1})	Ratio	$\mathcal{F}$	Fraction GT
^{60}Co	6.03E−04	1.27E−02	1.27E−07	1.15E−02	1.11E+00	1	7.25E−01
^{59}Co	1.14E−02	6.57E−04	1.27E−07	5.44E−04	1.21E+00	2	5.33E−01
^{54}Mn	2.30E−04	1.57E−02	6.68E−08	8.86E−03	1.77E+00	4	4.03E−03
^{64}Cu	7.37E−06	3.69E−01	4.25E−08	...	...	...	9.41E−01
^{61}Ni	1.46E−03	1.20E−03	2.86E−08	...	...	...	5.47E−01
^{63}Cu	5.16E−05	1.86E−02	1.53E−08	...	...	...	7.50E−01
^{58}Co	2.79E−05	3.07E−02	1.48E−08	1.55E−02	1.98E+00	11	4.76E−02
^{53}Mn	8.08E−05	8.97E−03	1.37E−08	6.81E−03	1.32E+00	7	6.69E−02
^{55}Fe	1.14E−04	6.00E−03	1.25E−08	1.21E−02	4.98E−01	5	6.11E−04
^{55}Mn	2.94E−02	2.25E−05	1.21E−08	2.03E−05	1.11E+00	6	4.45E−03
^{57}Co	3.84E−05	1.29E−02	8.67E−09	1.04E−02	1.24E+00	12	1.45E−01
^{57}Fe	1.19E−02	1.84E−05	3.82E−09	4.83E−05	3.81E−01	8	6.19E−05
^{62}Cu	5.08E−08	4.60E+00	3.77E−09	...	...	...	9.86E−01
^{51}V	5.93E−03	2.96E−05	3.45E−09	1.08E−05	2.76E+00	14	2.44E−03
^{56}Mn	7.03E−04	2.56E−04	3.22E−09	4.29E−05	5.97E+00	17	7.08E−05
^{50}V	5.32E−06	2.45E−02	2.60E−09	3.05E−03	8.00E+00	18	1.55E−08
^{56}Fe	8.30E−02	1.31E−06	1.93E−09	2.81E−05	4.66E−02	3	4.46E−03
^{60}Ni	3.36E−03	2.74E−05	1.53E−09	1.39E−04	1.97E−01	9	4.95E−01
^{51}Cr	7.44E−06	9.33E−03	1.36E−09	5.20E−03	1.80E+00	16	1.02E−09
^{53}Cr	2.06E−02	2.46E−06	9.57E−10	1.63E−05	1.51E−01	13	2.60E−05

$\dot{Y}_e^{tot}$ = −4.96E−07 s^{-1}, $\dot{Y}_e^{tot}$(FFN) = −3.97E−07 s^{-1}

NOTE.—Columns are as explained in Table 4.

TABLE 6

LIST OF NUCLEI

(ELECTRON CAPTURE: ρ = 1.06E+09, T_9 = 4.93E+00, Y_e = 0.43000)

^AZ	X_k	λ_k^{ec} (s^{-1})	$\lvert \dot{Y}_e^{ec}(k) \rvert$ (s^{-1})	λ_k^{ec} FFN (s^{-1})	Ratio	$\mathcal{F}$	Fraction GT
^{60}Co	9.51E−05	2.31E+00	3.66E−06	2.31E+00	9.99E−01	1	9.56E−01
^{66}Cu	1.31E−04	6.56E−01	1.30E−06	...	...	...	8.36E−01
^{62}Co	1.03E−03	3.22E−02	5.34E−07	...	...	...	7.02E−01
^{68}Cu	8.35E−04	2.62E−02	3.21E−07	...	...	...	2.61E−01
^{56}Mn	5.62E−04	2.90E−02	2.91E−07	9.29E−03	3.12E+00	4	6.06E−03
^{52}V	7.40E−04	1.81E−02	2.58E−07	6.11E−03	2.96E+00	5	2.06E−03
^{59}Co	4.42E−05	3.35E−01	2.51E−07	4.35E−01	7.71E−01	2	9.04E−01
^{61}Co	6.60E−03	2.23E−03	2.42E−07	...	...	...	6.70E−01
^{67}Cu	6.34E−03	2.38E−03	2.26E−07	...	...	...	2.65E−01
^{65}Cu	1.84E−04	5.91E−02	1.67E−07	...	...	...	7.05E−01
^{51}V	8.05E−04	9.71E−03	1.53E−07	4.40E−03	2.21E+00	8	4.45E−02
^{48}Sc	5.93E−05	8.25E−02	1.02E−07	3.82E−04	2.16E+02	23	1.10E−07
^{64}Cu	5.41E−07	1.10E+01	9.34E−08	...	...	...	9.72E−01
^{63}Ni	1.33E−03	3.87E−03	8.15E−08	...	...	...	6.45E−01
^{55}Mn	4.85E−04	8.73E−03	7.70E−08	9.10E−03	9.60E−01	6	7.29E−02
^{58}Mn	1.44E−03	2.94E−03	7.30E−08	3.16E−04	9.30E+00	15	6.51E−01
^{57}Mn	8.95E−03	4.03E−04	6.33E−08	2.36E−05	1.71E+01	19	6.68E−01
^{59}Fe	1.46E−02	1.83E−04	4.51E−08	1.49E−04	1.23E+00	10	6.61E−01
^{49}Ti	1.18E−04	1.70E−02	4.09E−08	3.02E−03	5.63E+00	16	2.82E−08
^{61}Ni	3.41E−06	5.07E−01	2.83E−08	...	...	...	9.16E−01

$\dot{Y}_e^{tot}$ = −8.21E−06 s^{-1}, $\dot{Y}_e^{tot}$(FFN) = −4.69E−06 s^{-1}

NOTE.—Columns are as explained in Table 4.

TABLE 7

LIST OF NUCLEI

(ELECTRON CAPTURE: ρ = 4.01E+10, T_9 = 7.33E+00, Y_e = 0.41000)

^AZ	X_k	λ_k^{ec} (s^{-1})	$\lvert \dot{Y}_e^{ec}(k) \rvert$ (s^{-1})	λ_k^{ec} FFN (s^{-1})	Ratio	$\mathcal{F}$	Fraction GT
^{58}Mn	9.84E−04	1.05E+03	1.79E−02	7.90E+02	1.33E+00	1	9.83E−01
^{61}Fe	6.09E−03	1.63E+02	1.63E−02	...	...	...	9.64E−01
^{49}Sc	1.39E−02	5.23E+01	1.48E−02	2.99E+01	1.75E+00	2	8.04E−01
^{63}Co	4.78E−03	1.62E+02	1.23E−02	...	...	...	9.57E−01
^{57}Mn	6.87E−04	8.36E+02	1.01E−02	4.29E+02	1.95E+00	5	9.84E−01
^{65}Ni	4.43E−03	1.44E+02	9.82E−03	...	...	...	9.34E−01
^{64}Co	2.56E−03	2.40E+02	9.62E−03	...	...	...	9.37E−01
^{55}V	5.46E−03	9.23E+01	9.16E−03	...	...	...	9.58E−01
^{53}V	2.76E−03	1.73E+02	9.01E−03	1.28E+02	1.36E+00	3	9.32E−01
^{59}Mn	3.16E−03	1.41E+02	7.53E−03	...	...	...	9.65E−01
^{60}Mn	1.49E−03	2.55E+02	6.32E−03	...	...	...	9.64E−01
^{57}Cr	5.92E−03	6.09E+01	6.32E−03	...	...	...	9.55E−01
^{59}Fe	5.06E−04	7.20E+02	6.17E−03	7.43E+02	9.69E−01	4	9.83E−01
^{62}Co	2.45E−04	1.44E+03	5.68E−03	...	...	...	9.81E−01
^{50}Sc	1.03E−02	2.55E+01	5.26E−03	...	...	...	5.56E−01
^{60}Fe	4.22E−03	6.73E+01	4.73E−03	1.44E+01	4.67E+00	7	9.60E−01
^{68}Cu	1.19E−03	2.22E+02	3.89E−03	...	...	...	8.57E−01
^{54}V	2.15E−03	9.66E+01	3.85E−03	...	...	...	8.50E−01
^{56}Cr	6.34E−03	3.33E+01	3.77E−03	...	...	...	9.50E−01
^{61}Co	1.80E−04	1.15E+03	3.39E−03	...	...	...	9.84E−01

$\dot{Y}_e^{tot}$ = −2.23E−01 s^{-1}, $\dot{Y}_e^{tot}$(FFN) = −4.72E−02 s^{-1}

NOTE.—Columns are as explained in Table 4.

TABLE 8

LIST OF NUCLEI

(BETA-DECAY: ρ = 5.86E+07, T_9 = 3.40E+00, Y_e = 0.47000)

^AZ	X_k	λ_k^{bd} (s^{-1})	$\lvert \dot{Y}_e^{bd}(k) \rvert$ (s^{-1})	λ_k^{bd} FFN (s^{-1})	Ratio	$\mathcal{F}$	Fraction GT
^{57}Fe	2.60E−04	1.10E−05	5.04E−11	3.71E−06	2.98E+00	2	9.97E−01
^{54}Mn	2.16E−04	8.81E−06	3.52E−11	1.57E−06	5.62E+00	4	3.06E−01
^{58}Co	1.31E−04	5.67E−06	1.27E−11	1.16E−06	4.87E+00	5	6.51E−01
^{53}Cr	7.36E−05	5.93E−06	8.22E−12	1.03E−05	5.76E−01	3	9.87E−01
^{60}Co	1.02E−07	4.66E−03	7.94E−12	1.09E−03	4.28E+00	8	3.37E−01
^{56}Mn	1.98E−08	1.09E−02	3.87E−12	3.82E−03	2.86E+00	11	2.89E−03
^{55}Mn	2.61E−04	3.68E−07	1.75E−12	3.01E−05	1.22E−02	1	2.93E−01
^{56}Fe	5.05E−01	1.19E−10	1.07E−12	2.25E−10	5.29E−01	6	9.99E−01
^{57}Co	3.55E−02	1.34E−09	8.36E−13	2.24E−09	5.99E−01	10	9.93E−01
^{59}Co	5.59E−04	8.11E−08	7.69E−13	1.48E−07	5.49E−01	9	8.03E−01
^{59}Fe	2.06E−09	6.95E−03	2.43E−13	5.11E−03	1.36E+00	14	9.83E−01
^{50}V	4.74E−07	1.89E−05	1.79E−13	4.03E−06	4.70E+00	16	1.32E−07
^{56}Co	5.56E−04	1.67E−08	1.66E−13	1.46E−08	1.15E+00	15	9.75E−01
^{58}Fe	8.28E−05	1.09E−07	1.55E−13	8.52E−07	1.28E−01	12	9.98E−01
^{52}V	4.32E−10	1.60E−02	1.33E−13	2.07E−03	7.70E+00	18	1.41E−03
^{55}Fe	5.20E−02	1.30E−10	1.23E−13	1.97E−10	6.63E−01	13	9.64E−01
^{61}Co	4.60E−09	1.36E−03	1.02E−13	...	...	...	9.58E−01
^{63}Ni	5.78E−09	3.16E−04	2.90E−14	...	...	...	9.98E−01
^{54}Cr	4.58E−06	2.90E−07	2.46E−14	2.19E−05	1.32E−02	7	9.82E−01
^{64}Cu	5.00E−09	1.34E−04	1.05E−14	...	...	...	9.76E−01

$\dot{Y}_e^{tot}$ = 1.24E−10 s^{-1}, $\dot{Y}_e^{tot}$(FFN) = 1.94E−10 s^{-1}

NOTE.—Columns are as explained in Table 4.

TABLE 9

LIST OF NUCLEI

(BETA-DECAY: ρ = 1.45E+08, T_9 = 3.80E+00, Y_e = 0.45000)

^AZ	X_k	λ_k^{bd} (s^{-1})	$\lvert \dot{Y}_e^{bd}(k) \rvert$ (s^{-1})	λ_k^{bd} FFN (s^{-1})	Ratio	$\mathcal{F}$	Fraction GT
^{59}Fe	4.17E−03	1.02E−02	7.19E−07	6.88E−03	1.48E+00	1	9.95E−01
^{61}Co	3.95E−03	1.90E−03	1.24E−07	...	...	...	9.85E−01
^{60}Fe	1.90E−03	3.33E−03	1.05E−07	7.95E−03	4.19E−01	2	1.00E+00
^{56}Mn	7.03E−04	7.99E−03	1.00E−07	2.52E−03	3.18E+00	6	1.42E−02
^{60}Co	6.03E−04	4.54E−03	4.56E−08	1.58E−03	2.88E+00	9	5.91E−01
^{52}V	1.17E−04	1.23E−02	2.77E−08	1.36E−03	9.02E+00	13	6.77E−03
^{55}Cr	5.85E−04	1.52E−03	1.61E−08	4.21E−03	3.59E−01	5	3.22E−01
^{57}Mn	6.72E−04	1.36E−03	1.60E−08	1.91E−02	7.09E−02	3	3.11E−03
^{53}V	9.45E−05	5.60E−03	9.99E−09	5.58E−03	1.00E+00	11	7.21E−04
^{62}Co	7.41E−06	7.87E−02	9.41E−09	...	...	...	3.44E−01
^{63}Ni	1.92E−03	3.02E−04	9.18E−09	...	...	...	9.98E−01
^{53}Cr	2.06E−02	1.57E−05	6.11E−09	2.74E−05	5.74E−01	10	9.95E−01
^{57}Fe	1.19E−02	2.65E−05	5.50E−09	9.14E−06	2.89E+00	16	9.99E−01
^{54}Cr	1.63E−01	1.61E−06	4.86E−09	4.69E−05	3.43E−02	4	9.96E−01
^{65}Ni	6.61E−05	4.06E−03	4.13E−09	...	...	...	9.16E−01
^{58}Fe	4.17E−01	4.96E−07	3.57E−09	4.25E−06	1.17E−01	7	9.99E−01
^{58}Mn	1.20E−06	1.71E−01	3.54E−09	1.30E−01	1.32E+00	15	2.48E−01
^{51}Ti	1.28E−04	1.07E−03	2.70E−09	1.55E−03	6.93E−01	12	2.86E−01
^{63}Co	6.93E−06	2.05E−02	2.26E−09	...	...	...	5.59E−01
^{61}Fe	1.31E−06	8.64E−02	1.85E−09	...	...	...	8.46E−01

$\dot{Y}_e^{tot}$ = 1.22E−06 s^{-1}, $\dot{Y}_e^{tot}$(FFN) = 1.29E−06 s^{-1}

NOTE.—Columns are as explained in Table 4.

TABLE 10

LIST OF NUCLEI

(BETA-DECAY: ρ = 1.06E+09, T_9 = 4.93E+00, Y_e = 0.43000)

^AZ	X_k	λ_k^{bd} (s^{-1})	$\lvert \dot{Y}_e^{bd}(k) \rvert$ (s^{-1})	λ_k^{bd} FFN (s^{-1})	Ratio	$\mathcal{F}$	Fraction GT
^{61}Fe	1.06E−02	1.25E−01	2.16E−05	...	...	...	9.87E−01
^{57}Cr	1.91E−03	3.31E−01	1.11E−05	2.15E+00	1.54E−01	1	9.77E−01
^{59}Mn	1.76E−03	3.50E−01	1.04E−05	1.00E+00	3.49E−01	3	9.59E−01
^{62}Fe	8.38E−03	6.38E−02	8.63E−06	...	...	...	9.99E−01
^{63}Co	1.69E−02	2.01E−02	5.40E−06	...	...	...	9.57E−01
^{67}Ni	2.11E−02	1.71E−02	5.38E−06	...	...	...	9.73E−01
^{58}Cr	4.99E−04	6.02E−01	5.18E−06	7.49E+00	8.03E−02	2	9.98E−01
^{58}Mn	1.44E−03	1.61E−01	3.98E−06	1.22E−01	1.31E+00	6	6.65E−01
^{50}Sc	1.74E−03	1.10E−01	3.82E−06	1.34E−02	8.23E+00	15	1.23E−02
^{65}Co	9.56E−04	1.85E−01	2.73E−06	...	...	...	7.51E−01
^{64}Co	5.68E−04	2.29E−01	2.03E−06	...	...	...	6.09E−01
^{54}V	8.33E−04	1.18E−01	1.82E−06	5.14E−02	2.29E+00	12	3.13E−02
^{65}Ni	3.87E−02	2.70E−03	1.61E−06	...	...	...	9.91E−01
^{51}Ti	2.91E−02	2.13E−03	1.22E−06	1.13E−03	1.88E+00	13	9.78E−01
^{62}Co	1.03E−03	7.16E−02	1.18E−06	...	...	...	7.98E−01
^{55}Cr	1.78E−02	3.31E−03	1.07E−06	6.05E−03	5.48E−01	9	9.82E−01
^{68}Ni	2.09E−02	2.84E−03	8.72E−07	...	...	...	9.93E−01
^{59}Fe	1.46E−02	3.50E−03	8.64E−07	1.31E−03	2.66E+00	16	9.98E−01
^{60}Fe	1.00E−01	3.63E−04	6.05E−07	6.82E−04	5.32E−01	11	9.99E−01
^{63}Fe	5.10E−05	7.18E−01	5.81E−07	...	...	...	8.75E−01

$\dot{Y}_e^{tot}$ = 9.57E−05 s^{-1}, $\dot{Y}_e^{tot}$(FFN) = 1.94E−04 s^{-1}

NOTE.—Columns are as explained in Table 4.

TABLE 11

LIST OF NUCLEI

(BETA-DECAY: ρ = 4.01E+10, T_9 = 7.33E+00, Y_e = 0.41000)

^AZ	X_k	λ_k^{bd} (s^{-1})	$\lvert \dot{Y}_e^{bd}(k) \rvert$ (s^{-1})	λ_k^{bd} FFN (s^{-1})	Ratio	$\mathcal{F}$	Fraction GT
^{52}Sc	1.24E−03	1.09E−03	2.59E−08	...	...	...	9.38E−01
^{62}Mn	1.53E−04	7.78E−03	1.92E−08	...	...	...	9.61E−01
^{56}V	5.16E−04	2.02E−03	1.87E−08	...	...	...	9.89E−01
^{53}Sc	5.70E−04	1.56E−03	1.68E−08	...	...	...	9.85E−01
^{51}Sc	1.08E−02	6.04E−05	1.28E−08	3.55E−04	1.70E−01	3	9.85E−01
^{57}V	3.77E−04	1.84E−03	1.22E−08	...	...	...	9.91E−01
^{60}Mn	1.49E−03	4.40E−04	1.09E−08	1.17E−02	3.77E−02	1	9.72E−01
^{51}Ca	3.13E−04	1.47E−03	9.06E−09	...	...	...	9.93E−01
^{55}Ti	4.97E−04	9.70E−04	8.77E−09	...	...	...	9.95E−01
^{68}Co	8.07E−04	6.98E−04	8.28E−09	...	...	...	0.00
^{61}Mn	2.65E−03	1.86E−04	8.08E−09	...	...	...	9.90E−01
^{49}Ca	3.88E−02	8.80E−06	6.97E−09	7.36E−05	1.20E−01	5	9.86E−01
^{50}Ca	7.68E−03	4.46E−05	6.85E−09	...	...	...	9.98E−01
^{55}V	5.46E−03	5.75E−05	5.71E−09	1.88E−03	3.06E−02	2	9.94E−01
^{59}Cr	8.58E−04	3.50E−04	5.09E−09	...	...	...	9.92E−01
^{63}Fe	2.42E−03	1.17E−04	4.49E−09	...	...	...	9.92E−01
^{53}Ti	1.28E−02	1.53E−05	3.71E−09	1.36E−04	1.12E−01	7	9.95E−01
^{54}Ti	4.17E−03	4.64E−05	3.58E−09	...	...	...	9.99E−01
^{50}Sc	1.03E−02	1.61E−05	3.32E−09	7.94E−05	2.03E−01	9	8.99E−01
^{66}Co	4.42E−03	3.43E−05	2.29E−09	...	...	...	0.00

$\dot{Y}_e^{tot}$ = 2.16E−07 s^{-1}, $\dot{Y}_e^{tot}$(FFN) = 8.38E−07 s^{-1}

NOTE.—Columns are as explained in Table 4.

effective rates yield a larger value for $|\dot{Y}_e|$ and the difference is increasing. This difference shows the effect of including $A > 60$ nuclei in the network. As Y_e drops, neutron rich nuclei such as ^{66,68}Cu, ^{62}Co, ^{61}Fe, ^{63}Co, ^{65}Ni, and others begin to make sizeable contributions to $\dot{Y}_e$, because of their increasing abundance.

In the case of beta-decay, $\dot{Y}_e$ calculated using the effective rates lags slightly behind the FFN estimate. The difference between the effective rate prediction and the FFN value increases with each successive point in the comparison. It can be seen in Table 10 that the effective rates underpredicted ^{58}Cr by a factor of roughly 12, and this single nucleus is the source of most of the difference between the two estimates of $\dot{Y}_e$ for this case. If ^{58}Cr were neglected in the FFN tabulation, $\dot{Y}_e$ would be roughly $1.3(-4)$ s^{-1}, much closer to the effective rate value. Table 11 exhibits this same trend, with the underprediction of ^{60}Mn ^{55}V, ^{57}Cr, and ^{58}Cr by the effective rates causing most of the difference in $\dot{Y}_e$. Indeed, if these nuclei were neglected, $\dot{Y}_e$ would be roughly $2.3(-7)$ s^{-1}, very close to the effective rate value. As will be discussed below, these differences in $\dot{Y}_e$ result from different input physics (Q-values), and these nuclei are not actually being "underpredicted" in the effective rates. Thus, the total $\dot{Y}_e$ due to electron capture and beta-decay estimated using the effective rates exhibits good agreement with the FFN estimates, when the input physics is consistent.

We now turn to detailed comparisons between the effective rates and the FFN rates. In general, the agreement between the two sets of electron capture rates is within roughly a factor of 2. This level of agreement is satisfying because it reassures us that the effective rates are fairly accurate in approximating the rates. The agreement with FFN is not perfect because the effective rates have treated the low-lying transitions in an overly simplistic fashion in their use of only the ground state to ground state transition. Several nuclei have effective electron capture rates which are quite different from the FFN values.

The nuclei ^{52}Mn, ^{50}V, and ^{48}Sc have effective electron capture rates which are roughly 4, 8, and 220 times, respectively, as strong as the FFN rates. Examination of their low-energy structure indicates that their ground state to ground state transitions are highly forbidden because of drastically different parent and daughter spins. The actual possible allowed transitions are energetically much less favorable. The effective rates have thus assumed much too strong a rate from low-lying transitions.

^{58}Mn and ^{60}Fe exhibit effective rates which are stronger than FFN by factors of roughly 9 and 5. The electron capture daughters of these neutron rich nuclei do not have measured masses, so that the electron capture Q-values have to be estimated with a mass formula. FFN used the Seeger & Howard (1975) formula, so that the Q-values used in the effective rates are quite different. This is not a problem in the effective rates; the input physics is different.

The effective electron capture rate for ^{59}Cu is roughly 7 times stronger than the FFN rate. This nucleus is similar to the case of ^{60}Cu discussed above and described in Figure 3. It could be that the FFN rate did not include the $2p_{3/2}$ resonant transitions as has been done here. This is the best explanation for the difference seen here. Again, this would be a case where the input physics is the source of the difference in the rates.

^{56}Fe and ^{53}Cr have effective electron capture rates which are 22 and 7 times weaker than the FFN rates. The effective rates are dominated by their ground state to ground state transitions, so that the source of the difference must be here. There are no obviously superallowed transitions in the actual spectra of these nuclei, but there are many possible low-lying transitions (in the case of ^{56}Fe electron capture, at least 199). We have been able to reproduce the FFN rates when a detailed calculation using all of these transitions is made. These nuclei are thus two cases where the simple approximation used for low-lying transitions has failed.

It can thus be seen that the effective electron capture rates are fairly good at predicting the actual electron capture rates to within a factor of 2. However, for five nuclei, ^{52}Mn, ^{50}V, ^{48}Sc, ^{56}Fe and ^{53}Cr, the approximation used for low-lying transitions failed. It is possible to determine when this failure leads to too strong a rate by examining the low-energy structure of the parent and daughter nuclei. If the parent and daughter spins are vastly different, and the effective rate is dominated by the ground state to ground state part of the rate, it is fairly certain that the effective rate is too strong. This technique will be used in examining the rankings of nuclei produced in the following sections. The case where the effective rate has drastically underestimated the actual rate is more worrisome, because such nuclei might not even show up in the lists produced. There is nothing we can do about this at present, except to take consolation from the fact that it only seems to happen rarely (two nuclei out of 80 here).

In the case of the beta-decays, the agreement between the effective rates and the FFN rates is not as good as in the electron capture case. The effective rates are usually within a factor of 5 of the FFN rates. This poorer agreement is a result of the phase space available for beta-decay, which makes the rate more sensitive to how the lower lying transitions are estimated.

Three nuclei, ^{54}Mn, ^{52}V, and ^{50}Sc, have been overpredicted by the effective rates. These nuclei have effective beta-decay rates which are roughly 6, 9, and 6 times, respectively, as large as the FFN rates. All three of these effective rates are dominated by the single low-energy state to ground state rate used here. Examination of their low-energy structure indicates that such transitions are highly forbidden. Thus the effective rates have overestimated the decay strength.

As was mentioned above in the discussion of the total $\dot{Y}_e$'s, the nuclei ^{60}Mn ^{55}V, ^{57}Cr, and ^{58}Cr have much weaker effective rates than their FFN rates. These neutron-rich nuclei do not have measured masses, so that the beta-decay Q-values have to be estimated with a mass formula. FFN used the Seeger & Howard (1975) formula, so that the Q-values used in the effective rates are quite different. This is not a problem in the effective rates; the input physics is different.

The largest class of differences between the effective decay rates and the FFN decay rates is the set of nuclei which have known Q-values but have much weaker effective rates than FFN rates. The nine nuclei which exhibit these characteristics are ^{55,57}Mn, ^{58}Fe, ^{54}Cr, ^{51}Sc, ^{49}Ca, and ^{52,53}Ti. These nuclei are too weak by factors of 80, 7, 8, 75, 5, 6, 8, 29, and 9, respectively. It appears that the effective rates are in error because of the treatment of the low-lying transitions. In fact, for several of the nuclei, these underpredictions occur at relatively high temperature, where more excited states in the parent nucleus are contributing to the rate. At lower temperatures, the same nu-

clei are actually overpredicted by the effective rates. A single ground state to ground state transition is not able to reproduce such varied behavior. Another possible source of error for the effective rates could be errors in calculating the partition functions. As can be seen in the second term of equation (31), the contribution of the back resonance to the decay rate is sensitive to the partition functions of the parent and daughter nuclei. Several of the nuclei listed above states of radically different spin near the parent or daughter ground states. The method used here for estimating partition functions can be in error in such cases.

Thus, the agreement between the effective decay rates and the FFN decay rates is not as good as in the electron case. The cases with different Q values are not a concern because different initial assumptions are being used in the rates. The cases of overprediction in the effective rates can be handled as they were in the electron capture case: check all nuclei dominated by low-lying transitions in any list of important nuclei. If a nucleus has highly mismatched parent and daughter spins, it has probably been overpredicted. As in the electron capture case, the underprediction of rates is a problem which is difficult to resolve. Such nuclei might not appear on a list. However, the number of nuclei with this problem is still relatively small. One confirmation of this fact is the total $\dot{Y}_e$. The effective rates yield a total $\dot{Y}_e$ which is close to the FFN $\dot{Y}_e$, albeit somewhat weaker.

In summary, this comparison of the effective rates with the FFN rates indicates that the effective rates are fairly successful at reproducing the FFN rates. The success is greater for electron capture than beta decay because of the greater sensitivity of the decays to low-lying transitions. We thus have confidence in the effective rates as a tool for probing weak interaction rates after core silicon burning.

4. GENERAL BEHAVIOR OF $\dot{Y}_e$

The rate of change in Y_e exhibits great sensitivity to temperature, density, and Y_e. This sensitivity will be seen in the trajectory which a star follows, but first we will examine the behavior by varying each parameter separately. The effects seen in the stellar trajectory will then be more understandable. Figure 5 shows the $\dot{Y}_e$ due to electron capture as a function of Y_e for two choices of temperature (T_9 = 3, 6.5) and density ($\rho = 10^8$ g cm^{-3}, 10^{10} g cm^{-3}). Figure 6 shows a similar plot for $\dot{Y}_e$ due to beta-decay. The effective rates used here and in the following sections have quenched GT strength functions.

Figure 5 shows that the electron capture $\dot{Y}_e$ decreases very quickly with decreasing Y_e, regardless of the temperature and density. The source of this dependence will be examined below. Another feature common to all choices of temperature and density is the fairly close agreement in $\dot{Y}_e$ using the effective rates and the FFN rates for larger values of Y_e, and the more rapid decrease in the FFN value with decreasing Y_e. This behavior is the result of the FFN tabulation using only nuclei with $A < 60$. As the NSE gas becomes more neutron rich, larger nuclei, considered for the first time here, begin to make large contributions to $\dot{Y}_e$. A third feature common to all choices of temperature and density is the "rippling" seen in $\dot{Y}_e$. In no case is the rate of change in Y_e a smooth function of Y_e; rather it appears to be a sum of peaks. These peaks show the effect of

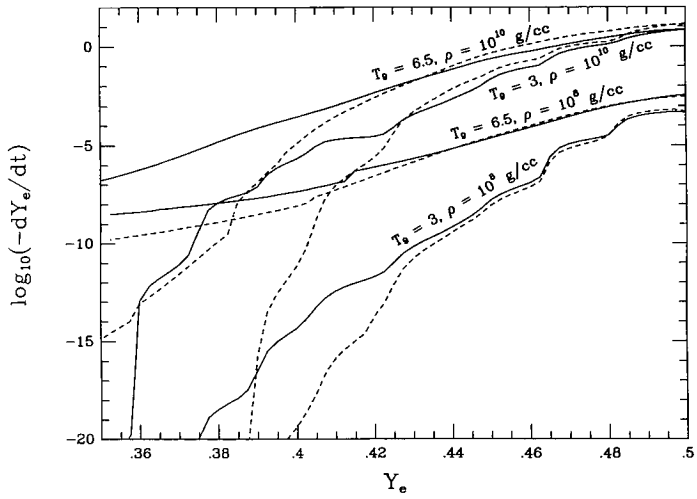

FIG. 5.—Logarithm of $\dot{Y}_e$ due to electron capture as a function of Y_e for several different temperatures and densities. For each choice of temperature and density, two $\dot{Y}_e$'s are plotted: the solid curve is the rate of change in Y_e due to the effective rates, while the dashed curve is the rate of change in Y_e due to the FFN rates.

various nuclei becoming abundant as Y_e approaches their Z/A value. As these nuclei become abundant, $\dot{Y}_e$ becomes dominated by them and it follows their abundance peak. An example of such a feature can be seen for the T_9 = 3 and $\rho = 10^8$ g cm^{-3} curve for $0.46 < Y_e < 0.48$. This peak is caused by ^{54,55}Fe, and ^{57}Co with charge to mass ratios of 0.481, 0.473, and 0.474, respectively. As Y_e drops below roughly 0.465, these nuclei become much less abundant and other nuclei become the dominant contributors to $\dot{Y}_e$.

The most striking feature of the electron capture case is the drastic drop in $\dot{Y}_e$ with Y_e. Depending on the temperature and density, the rate of change in Y_e drops by 5 to 20 orders of magnitude. The source of this large change is the effect which

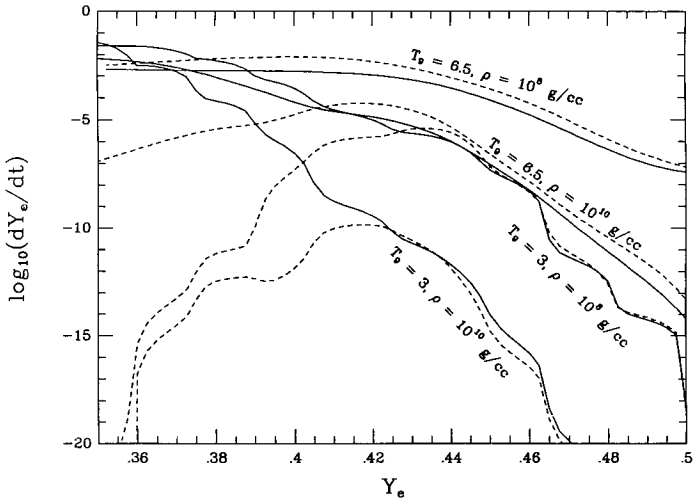

FIG. 6.—Logarithm of $\dot{Y}_e$ due to beta-decay as a function of Y_e for several different temperatures and densities. For each choice of temperature and density, two $\dot{Y}_e$'s are plotted: the solid curve is the rate of change in Y_e due to the effective rates, while the dashed curve is the rate of change in Y_e due to the FFN rates.

Y_e has on the NSE distribution of nuclei. As Y_e drops, the more abundant nuclei become more neutron-rich and their mass differences become larger. Thus, the electron capture Q-values become less favorable. This effect is illustrated in Figure 7*a*, where we have plotted the average electron capture Q-value as a function of Y_e. In this plot, we have computed the ground state to ground state electron capture Q-values of the 15 nuclei which make largest contributions to $\dot{Y}_e$ and averaged them. As can be seen, the points become increasingly negative with decreasing Y_e. The dominance of particular groups of nuclei can also be seen in the steps which Q^{ec}_{ave} takes as Y_e decreases.

The phase space integral is extremely sensitive to such changes in Q-values, and results in the large changes in $\dot{Y}_e$. This point is illustrated in Figure 7*b*, where $\dot{Y}_e/[\ln 2 \times \phi(\rho, T, Y_e, Q^{fit})]$ is plotted as a function of Y_e. (We have used $Z = 26$ and $A = 60$ in the Fermi function.) The quantity Q^{fit} is the parabolic fit to the Q-value which is plotted in Figure 7*a*. Over the range of Y_e plotted in Figure 5, $\dot{Y}_e$ varies by roughly 40 orders of magnitude (20 of which are not shown in the figure). After the phase space integral is divided out, the remaining physics in the function exhibits much smaller variations. The rapid change for $Y_e > 0.46$ is the result of $\dot{Y}_e$ being dominated by a few, more abundant, nuclei in these regimes. For Y_e near 0.50, ^{56}Ni, the most abundant nucleus, has a mass fraction of $\approx$0.99. The dominant nuclei just above $Y_e = 0.46$ have mass fractions on the order of 10^{-2}. Below this Y_e-value, the mass factions average roughly 10^{-4}. Thus it can be seen that the phase space integral accounts for most of the changes in $\dot{Y}_e$, with abundance changes accounting for much of the rest.

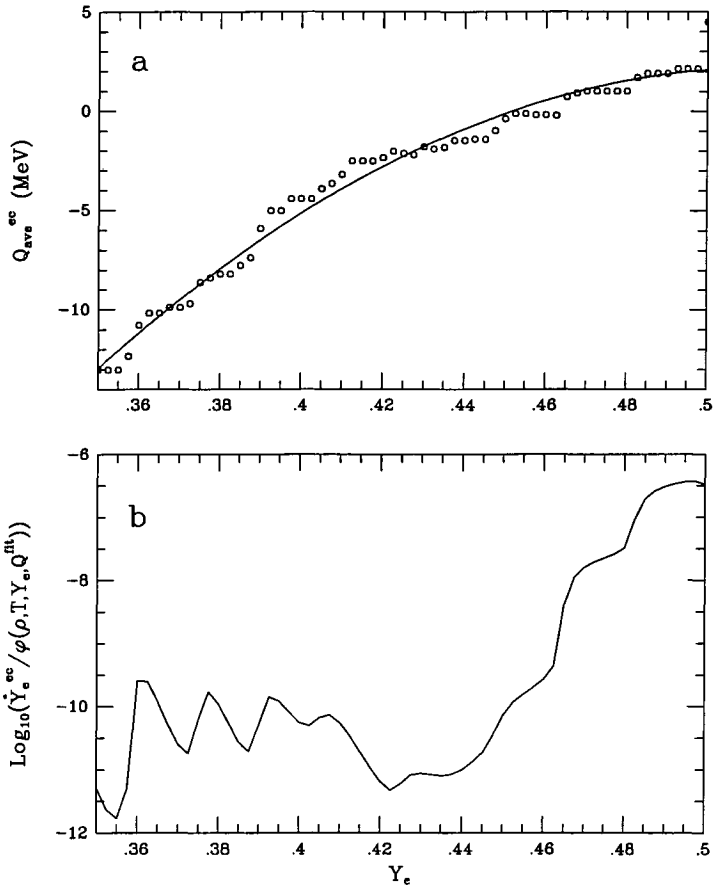

FIG. 7.—Study of the dependence of the electron capture $\dot{Y}_e$ on Q-values. (*a*) Average electron capture Q-value as a function of Y_e. The points are the average electron capture Q-values for $T_9 = 3$, $\rho = 10^8$ g cm^{-3}, while the solid curve is the fit to this set. (*b*) Variation of $\dot{Y}_e$, once the phase space space factor has been removed.

Returning to Figure 5, it can also be seen that $\dot{Y}_e$ is very sensitive to μ_e. A change in density from 10^8 to 10^{10} g cm^{-3} results in μ_e increasing from roughly 1.8 to 8.8 MeV, which leads to at least four orders of magnitude increase in $\dot{Y}_e$. The source of this effect is that increasing the density increases the number of electrons able to make transitions. Increasing the density also changes the character of the rates. The values of $\dot{Y}_e$ which follow the $T_9 = 3$, $\rho = 10^8$ g cm^{-3} curve are dominated by the ground state to ground state transition in the effective rates. For both of the $\rho = 10^{10}$ g cm^{-3} curves, $\dot{Y}_e$ is dominated by transitions to the GT resonance. This can be seen because the effective $\dot{Y}_e$ is consistently less by a factor of 2 than the FFN $\dot{Y}_e$, for large Y_e. It can also be seen in the fact that the $\rho = 10^{10}$ g cm^{-3}, $T_9 = 3$ and $T_9 = 6.5$ curves converge as $Y_e \rightarrow 0.5$. At $Y_e = 0.5$, ^{56}Ni dominates $\dot{Y}_e$, so that the lack of temperature dependence in both the effective and FFN cases indicates that the capture to the resonance is dominant.

Temperature affects $\dot{Y}_e$ in two ways. Firstly, increasing the temperature broadens the Fermi-Dirac distribution of electrons, increasing the number of electrons which are able to participate in transitions. This broadening can soften sensitivity to Q-values seen above. These effects can be seen by comparing the $\rho = 10^{10}$ g cm^{-3} curves. The downward trend in $\dot{Y}_e$ exhibited in the $T_9 = 6.5$ curve is much shallower than in the $T_9 = 3$ curve.

The second effect is a result of temperature induced changes on the NSE distribution. The higher the temperature, the higher the abundance of free protons. In some cases, the temperature can be high enough that $\dot{Y}_e$ is dominated by electron captures on free protons. The $T_9 = 6.5$, $\rho = 10^8$ g cm^{-3} curve is an example. The decrease in $\dot{Y}_e$ is four orders of magnitude from $Y_e = 0.5$ to 0.415. This decrease matches the decrease of proton mass fraction from 2.5×10^{-2} to 4.6×10^{-6}. Below $Y_e = 0.415$, free protons are no longer one of the 150 most abundant species, and they are no longer included in $\dot{Y}_e$. This is the cause of the sharp drop in $\dot{Y}_e$ just below $Y_e = 0.415$. Thus, below $Y_e = 0.415$, the value for $\dot{Y}_e$ is no longer accurate since the free protons are not included. No effort has been made to deal with this problem, since it is not encountered under stellar evolution conditions, where the temperature is only high when the density is much greater. However, an extension of this study to core collapse would need to include free protons at all times.

Figure 6 illustrates that $\dot{Y}_e$ due to beta decay exhibits many features similar to what was seen above with electron capture. The effective rates and the FFN rates yield values for $\dot{Y}_e$ which agree at higher Y_e, but diverge as Y_e drops. This divergence is again the result of the effective rates including nuclei with $A >$ 60. The "rippling" of $\dot{Y}_e$ discussed above for electron capture is again present here, for the low-temperature cases. As above, the ripples represent the ebb and flow of $\dot{Y}_e$ as various nuclei become more and then less abundant. The lack of ripples in the $T_9 = 6.5$ cases will be discussed below.

As was the case for electron capture, $\dot{Y}_e$ due to decays exhibits drastic changes with Y_e, but in this case $\dot{Y}_e$ increases with decreasing Y_e. Again, this behavior is mainly the effect of changes in the beta-decay Q-values. Figure 8*a* illustrates shows how the average beta decay Q-value becomes more favorable with decreasing Y_e, for the $T_9 = 3$, $\rho = 10^8$ g cm^{-3} case. As was done with the electron capture case, the nuclei which make the 15 largest contributions to $\dot{Y}_e$ have been used in the average. It can be seen that the Q-values become more positive with decreasing Y_e, again because the more neutron-rich nuclei have larger mass differences, and the strongest beta-decays induce transitions to more tightly bound nuclei. The beta-decay phase space integral is extremely sensitive to these Q-values. In Figure 8*b* this dependence is divided out of $\dot{Y}_e$ by forming $\dot{Y}_e/[\ln 2 \times \xi(\rho, T, Y_e, Q^{\rm fit})]$. The parabolic fit to the average Q-values, $Q^{\rm fit}$, is used in the decay phase space integral and is shown in Figure 8*a*. As can be seen in Figure 8*b*, the phase space integral appears to be the source of most of the large variations in $\dot{Y}_e$. For Y_e greater than roughly 0.46, this method fails because the average decay Q-value is becoming less than 0.511 MeV, at which point $\xi \rightarrow 0$. When $Q^{\rm fit}$ drops below 0.95 MeV, we have fixed $Q^{\rm fit}$ to have a value of 0.95 MeV. The more rapid drop in $\dot{Y}_e$ at larger values of Y_e indicates that ξ (and thus $Q^{\rm fit}$) should be smaller. Also, as Y_e approaches 0.5, the number of nuclei contributing to $\dot{Y}_e$ is smaller and details of individual become more important. It is more difficult to lump all of the phase space dependence into one factor.

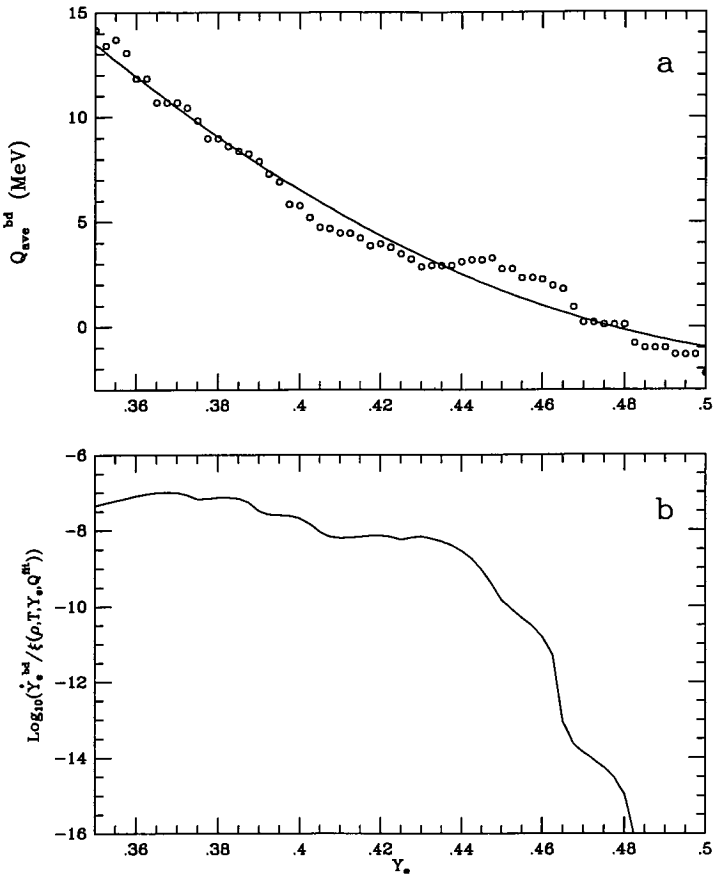

FIG. 8.—Study of the dependence of the beta-decay $\dot{Y}_e$ on Q-values. (*a*) Average beta-decay Q-value as a function of Y_e. The points are the average beta decay Q-values for $T_9 = 3$, $\rho = 10^8$ g cm^{-3}, while the solid curve is the fit to this set. (*b*) Variation of $\dot{Y}_e$, once the phase space space factor has been removed.

Figure 6 illustrates the great sensitivity of $\dot{Y}_e^{\rm bd}$ to density. For $T_9 = 3$, there is a six order of magnitude drop in $\dot{Y}_e$ as density increases from 10^8 g cm^{-3} to 10^{10} g cm^{-3}. This drop is due to the sensitivity of the beta-decay phase space integral to the electron chemical potential. As density increases, it becomes more and more difficult to place the electron emitted in such a decay into the highly degenerate gas of electrons. At $T_9 = 6.5$, the difference between $\dot{Y}_e$ for the two densities is not as large, because the Fermi-Dirac distribution of degenerate electrons has a much broader spread due to the high temperature.

As the temperature changes, the character of the decay rates changes. In the high-temperature cases, the decay rates are dominated by thermal population of the GT back resonance. This effect can be seen in $\dot{Y}_e$ plotted for both densities because the FFN value is roughly twice as large as the effective value. This is again a result of the effective rates being quenched by a factor of 2.

Another interesting feature of this figure is the difference between the effective $\dot{Y}_e$ and the FFN $\dot{Y}_e$ for $T_9 = 3$, $\rho = 10^{10}$ g cm^{-3} near $Y_e = 0.455$. Because the density is so high, the effective rates are dominated by decays through the GT back resonance. The large electron chemical potential blocks the low-energy transition in the effective rate. The decay from the back resonance, although decreased by the Boltzmann factor, has a large Q-value and thus has a much larger phase space factor. The effective $\dot{Y}_e$ is larger than the FFN value probably because of inaccuracies in estimating the partition functions of the parent and daughter nuclei, in particular ^{56,58}Mn. It is not possible to say more, because nothing has been published about the FFN partition functions, so that no comparison can be made.

A last feature of the effective $\dot{Y}_e$ curves which deserves comment is the fact that all four cases tend to asymptote to similar values at low Y_e. Two factors are causing this trend. First, Figure 8*a* demonstrates the decay Q-values are very large at low Y_e. The phase space integrals are thus less sensitive to changes in temperature or density. Second, the nuclei which are dominating $\dot{Y}_e$ at this point are extremely neutron-rich and are no longer in the *fp* shell. Thus the only part of the rate being used is the low-energy piece, which is being dominated by the large Q-values.

5. FOLLOWING A STELLAR TRAJECTORY

Although the general dependence of these rates on temperature, density, and electron fraction is interesting, it does not necessarily shed much light on which nuclei will be important in stellar evolution. During its evolution a presupernova star follows a complicated trajectory in ρ, T, and Y_e space in response to the physical processes occurring in the core, such as nuclear burning, neutrino emission, convection, and weak reactions. The temperature, density and electron fraction will vary at the same time. Thus none of the cuts which we made in ρ, T, and Y_e space in § 4 characterize a stellar trajectory. In this section, we construct a typical stellar trajectory for the center of the star, use it to set ρ, T, and Y_e as inputs to our code, and examine which nuclei become important.

It would seem to be difficult to construct a "typical" stellar trajectory because Type II progenitors are thought to come from stars in the relatively large range of $\sim 12\ M_\odot$ to $30\ M_\odot$. One might expect the central ρ, T, and Y_e to be a sensitive function of the amount of mass outside the core. However, these cores are extremely efficient thermostats and the late stages of evolution in the core are quite similar from one star to another. One example of this effect is the mass of the iron core, prior to collapse. Stars throughout this mass range tend to collapse with iron cores of $\sim 1.4\ M_\odot$, with deviations of only 20%. One could thus hope that the trajectories at these late times are also similar.

Figures 9*a* and 9*b* confirm this hope. We have plotted the central density and temperature as functions of Y_e, for 15, 18, and 25 $M_\odot$ stars evolved with the KEPLER stellar evolution code (Weaver, Zimmerman, & Woosley 1978). The KEPLER code presently uses the FFN electron capture rates (Weaver et al. 1985), but only Hansen (1966, 1968) and Mazurek et al. (1974; Mazurek 1973) beta-decay rates. It has long been argued that electron capture rates dominate the decay rates and choice of decays is thus irrelevant. As can be seen, all three stars follow similar trajectories. We have fit this trajectory by the following curves

$$\log_{10}\rho(Y_e) = 603 - 3642Y_e + 7439Y_e^2 - 5075Y_e^3\,,$$
$$T_9(Y_e) = 1212 - 7571Y_e + 15831Y_e^2 - 11047Y_e^3 \qquad (33)$$

and they are shown in Figures 9*a* and 9*b*.

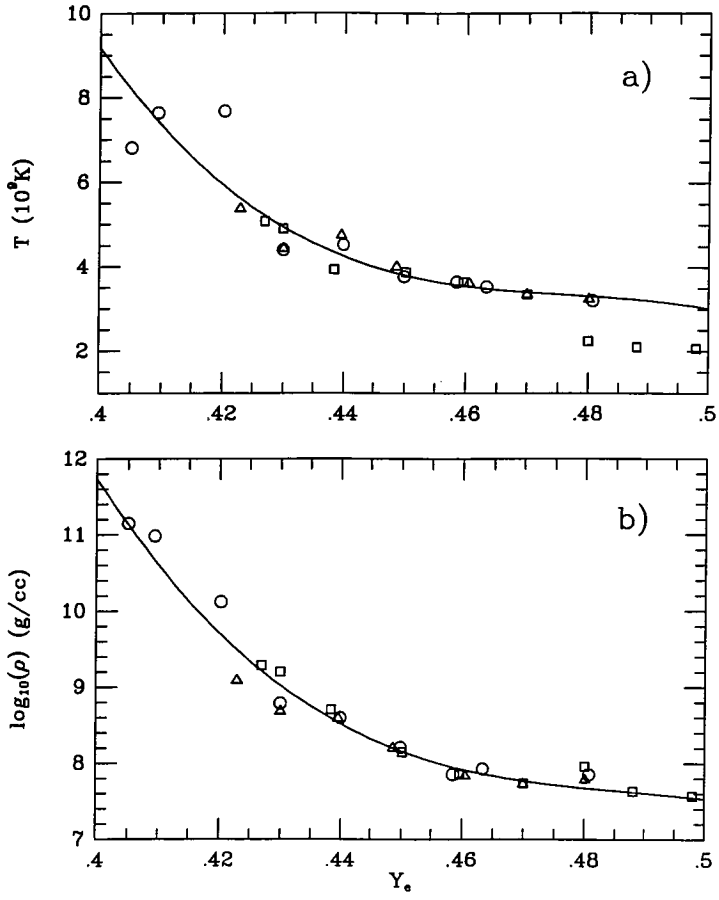

FIG. 9.—Stellar trajectories for (*a*) temperature and (*b*) density as a function of Y_e. The triangles are from a 15 $M_\odot$ star, the squares are from an 18 $M_\odot$ star, while the circles are from a 25 $M_\odot$ star. The solid curve in each plot is the fit listed in eq. (33).

Because our code includes nuclei not in the FFN tabulation, and uses the FFN approach to compute beta-decay rates, it is not strictly consistent to follow this trajectory with our code. The inclusion of these new rates might have affected Y_e, altering the relationship between ρ, T, and Y_e. Better consistency could be achieved if our code were incorporated into a one zone model (Fuller 1982), or, better, into a stellar evolution code. Such studies are beyond the scope of this paper. Here we only wish to know which nuclei could be important along this trajectory. If, at some point, $\dot{Y}_e$ is dominated by either $A > 60$ nuclei or beta decays, the trajectory is no longer self-consistent and this new physics could be important in presupernova evolution.

In what follows, we have calculated abundances and weak interaction rates at many points along the stellar trajectory. This trajectory has been followed for $0.40 \le Y_e \le 0.50$, in steps of $\Delta Y_e = 0.00125$. At each point along the trajectory, the abundances and rates have been sorted and saved. A similar calculation has been done using only the FFN rates. It is from this database that the rest of the results in this section are obtained.

Figures 10 and 11 show $\dot{Y}_e$ due to electron capture and beta-decay along the trajectory. The evolution begins at large Y_e and proceeds to the left. For $Y_e > 0.485$, this calculation is not relevant because in the core, silicon burning has not yet finished and it is not valid to assume NSE. It can be seen from Figure 10 that $\dot{Y}_e$ due to electron captures agrees quite well with the FFN $\dot{Y}_e$. This provides further assurance that the effective rates are reproducing the FFN rates fairly accurately when comparisons are possible. The FFN $\dot{Y}_e$ is roughly 40% stronger than the effective $\dot{Y}_e$ for Y_e near 0.48 and 0.44. This difference is due to the quenched GT strength used in the effective rates. As will be seen below, ^{55}Co and ^{60}Co, respectively, are the dominant nuclei here and more than half of their strength comes from captures to the resonant GT strength. Near Y_e of 0.425, the FFN $\dot{Y}_e$ becomes weaker than the effective $\dot{Y}_e$ because of the intrusion of $A > 60$ nuclei. By Y_e of 0.40, the effective $\dot{Y}_e$ is roughly a factor of 10 stronger than the FFN case.

Figure 11 shows similar agreement between the FFN and effective $\dot{Y}_e$ due to beta-decays. It can be seen that the FFN $\dot{Y}_e$ is always larger than the effective value. This is again a result of the effective rates using quenched GT resonances. There is a factor of 4.5 difference between the $\dot{Y}_e$'s at Y_e near 0.425. This difference is due the neutron rich nuclei ^{55}V, ^{57,58}Cr, and ^{59}Mn, whose beta-decay Q-values are not known. As discussed above, FFN used the Seeger & Howard (1975) mass formula in these cases and these Q-values are much different from the values obtained with the Comay et al. (1988) mass law. The significant deviations in the FFN $\dot{Y}_e$ below $Y_e \approx 0.406$ are due to the nuclei ^{45,46}Ar and ^{49}K, which also have no measured Q-values.

The general trend for $\dot{Y}_e$ as a function of Y_e seen in Figures 10 and 11 is similar to what was seen in Figures 5 and 6, for large Y_e. At large values of Y_e, the electron capture $\dot{Y}_e$ de-

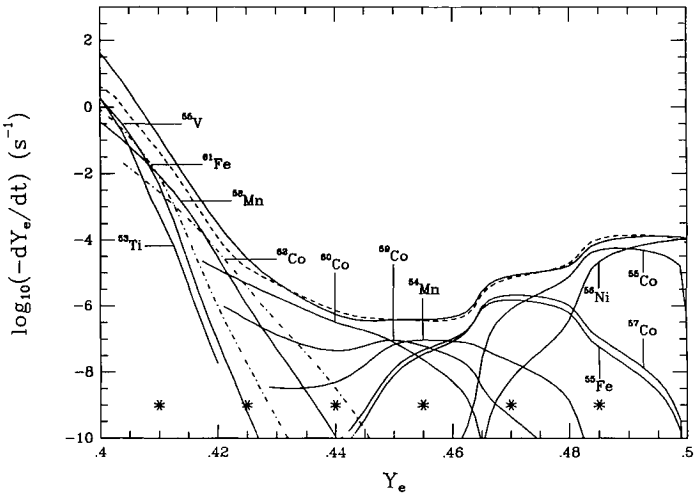

FIG. 10.—Variation of $\dot{Y}_e$ due to electron capture along the stellar trajectory. The dashed and uppermost solid curves are the total $\dot{Y}_e$'s due to electron capture obtained using the FFN and effective rates, respectively. The $\dot{Y}_e$'s due to the nuclei which have the strongest $\dot{Y}_e$ at each point are also plotted using solid curves if $A \leq 60$, and dash-dotted curves if $A > 60$. The effective rates are used for each of these nuclei. The asterisks (*) show where along the trajectory a ranking of important nuclei has been made.

creases drastically with Y_e, while the beta-decay $\dot{Y}_e$ increases even more drastically with Y_e. However, as Y_e decreases along the trajectory, these trends stop and actually reverse. The reason for this behavior is the increase in temperature and density which accompanies the drop in Y_e along this trajectory. Figure 12 illustrates how the electron chemical potential evolves along the trajectory. The average electron capture and beta decay Q-values along this trajectory are plotted for comparison. As was seen above, the beta-decay Q-values increase as Y_e decreases, while the electron capture Q-values become more

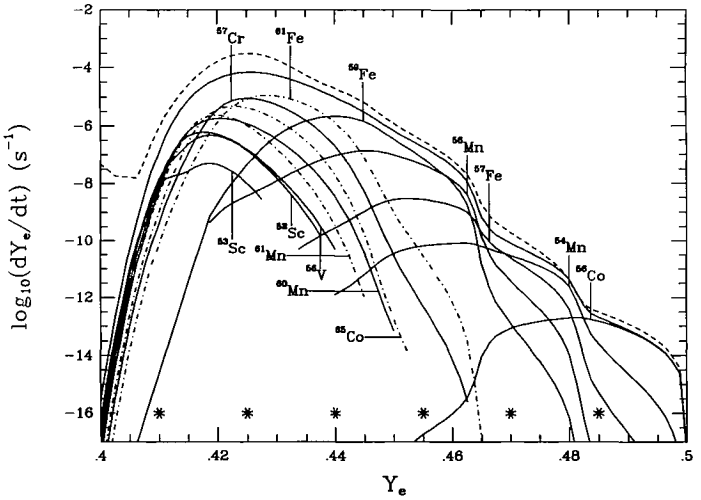

FIG. 11.—Variation of $\dot{Y}_e$ due to beta decay along the stellar trajectory. The dashed and uppermost solid curves are the total $\dot{Y}_e$'s due to beta decay obtained using the FFN and effective rates, respectively. The $\dot{Y}_e$'s due to the nuclei which have the strongest $\dot{Y}_e$ at each point are also plotted using solid curves if $A \leq 60$, and dash-dotted curves if $A > 60$. The effective rates are used for each of these nuclei. The asterisks (*) show where along the trajectory a ranking of important nuclei has been made.

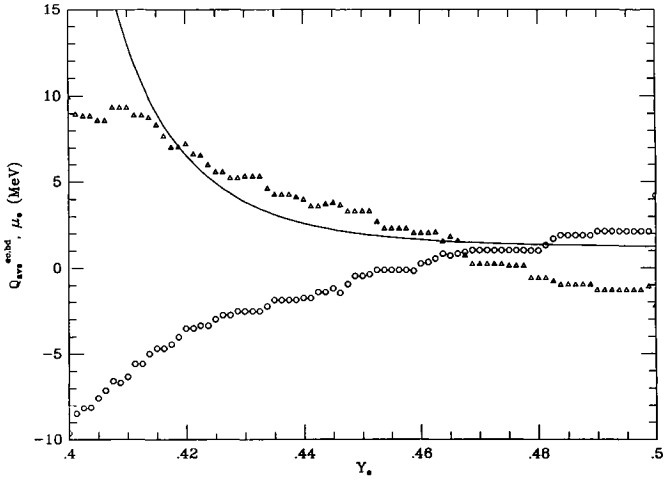

FIG. 12.—Comparison of electron chemical potential, μ_e, and average electron capture and beta-decay Q-values along the stellar trajectory. The solid curve shows the evolution of μ_e. The triangles show the average beta decay Q-values, while the circles show the average electron capture Q-values.

negative as Y_e decreases. The effect of these changes in Q-values explains the behavior of $\dot{Y}_e$ for large values of Y_e. As Y_e decreases, the electron chemical potential increases. This increase indicates a growing number of electrons with large degeneracy energies, which are available for electron capture and to block beta-decays. Using Figures 10 and 12, it can be seen that the trend in the electron capture $\dot{Y}_e$ changes when μ_e becomes larger than the magnitude of the average electron capture Q-value, thus compensating for the less favorable Q-values. Likewise, the trend in the beta-decay $\dot{Y}_e$ changes when μ_e becomes larger than the beta-decay Q-value, thus blocking most of the decay phase space.

Figures 10 and 11 also exhibit the "ripples" which were discussed in § 4. In these plots, the $\dot{Y}_e$ of the nuclei which make the largest contribution to $\dot{Y}_e$ are also plotted. The source of the rippling can be seen in the sudden decreases in $\dot{Y}_e$ made by these nuclei as their abundance changes abruptly. It is also interesting to note that, except for Y_e near 0.5, no single nucleus contributes more than 65% to the total change in $\dot{Y}_e$. This can be seen by the fact that the total $\dot{Y}_e$ plotted in both Figures 5 and 6 is clearly larger than the $\dot{Y}_e$ for each most important nucleus. As Y_e drops, the effect becomes stronger as a larger and larger number of nuclei begin to make a significant contribution to $\dot{Y}_e$. These figures also show where $A > 60$ nuclei begin to make significant contributions to $\dot{Y}_e$. By $Y_e \approx 0.44$, $\dot{Y}_e$ due to beta-decay is dominated by its first $A > 60$ nucleus, ^{61}Fe. For $\dot{Y}_e$ due to electron capture, the first such nucleus, which dominates at $Y_e \approx 0.425$, is ^{62}Co.

It is also interesting to ask how much of the effective electron capture and beta-decay rates are being contributed by transitions involving the GT resonances discussed in §§ 3.1 to 3.3. In Figure 13 the fraction of $\dot{Y}_e$ due to these resonant transitions is plotted. This fraction is computed in the following manner at each ρ, T, and Y_e point:

$$\text{Fraction GT} = \sum_k \frac{\dot{Y}_e^{\text{ec(bd)}}(k)}{\dot{Y}_e^{\text{ec(bd)}}(\text{total})} X_{\text{GT}}^{\text{ec(bd)}}(k) , \qquad (34)$$

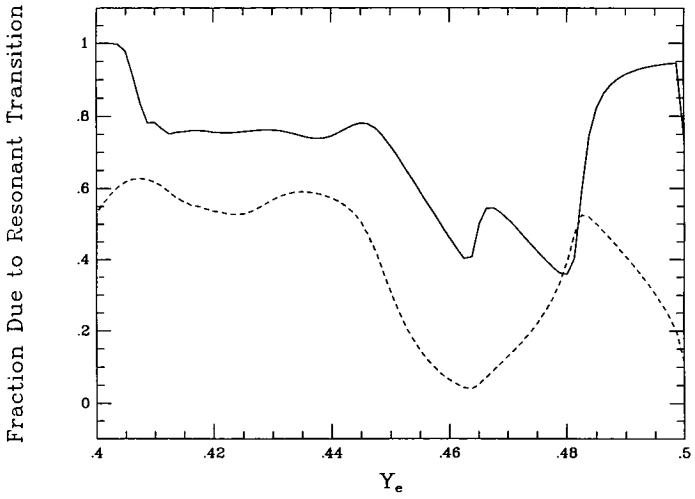

FIG. 13.—Fraction of total $\dot{Y}_e$ caused by transitions occuring through the GT resonance as a function of Y_e along the stellar trajectory. The solid curve shows the fraction of the beta-decay $\dot{Y}_e$ due to GT resonances. The dashed curve shows the fraction of the electron capture $\dot{Y}_e$ due to GT resonances.

where $X_{\rm GT}^{\rm ec(bd)}(k)$ is the fraction of the change in Y_e due to electron capture (beta-decay) on the kth nucleus which proceeds through the GT resonance. For Y_e above roughly 0.44, roughly 25% of the $\dot{Y}_e$ due to electron capture is contributed by captures to the GT resonance (the peak near 0.4825 is due to ^{55}Co, which is 74% GT). Below $Y_e \approx 0.44$, the fraction of electron capture $\dot{Y}_e$ due to the resonant transition increases to roughly 60%, because μ_e is increasing so quickly. The curve for beta-decay is striking because it indicates that much of the decays are proceeding through the thermal excitation of the back resonance throughout the stellar trajectory. Initially the fraction is high because the beta-decay $\dot{Y}_e$ is dominated by ^{56}Co, whose decay rate is dominated by the decay of its back resonance at the 97% level. As Y_e decreases, the fraction of the beta-decay $\dot{Y}_e$ contributed by the back resonance increases to almost 100%. This dominance occurs for two reasons. Firstly, temperature increases as Y_e decreases, making the thermal population of the back resonance easier. Also, as μ_e increases, the increasing blockage of beta-decay phase space favors transitions with large Q-values, such as the back resonant transitions. This figure thus shows that, under the conditions encountered in stellar evolution, the beta-decays are even more sensitive to the treatment of the GT resonance than the electron captures are.

As Figures 10 and 11 show, the most important electron capture and beta-decay nuclei change as the conditions of the trajectory change. Thus we have chosen six points along the trajectory to examine in greater detail, in order to prioritize which nuclei make the largest contribution to $\dot{Y}_e$ under each set of conditions. These points are at $Y_e = 0.485, 0.470, 0.455, 0.440, 0.425$, and 0.410, and are marked by asterisks (*) in Figures 10 and 11. Each point has been chosen to lie in the center of a "ripple" seen in the evolution of $\dot{Y}_e$. Hereafter, we will denote the Y_e-values at these points by the symbol Y. No points with Y_e greater than 0.485 have been chosen because the star has not yet completed core silicon burning under such conditions and an NSE estimate of the abundances is not relevant. No points lower than $Y_e = 0.41$ have been considered because this is too high a density for the current treatment.

We seek the nuclei which make the largest contribution to $\dot{Y}_e$ throughout the trajectory, not just at the points chosen above. Thus, we have computed a ranking parameter $\mathcal{R}$, given by the average fraction of $\dot{Y}_e$ contributed by each nucleus for Y_e-values within 0.0075 of each Y:

$$\mathcal{R} = \left\langle \frac{\dot{Y}_e^{\rm ec(bd)}(k)}{\dot{Y}_e^{\rm ec(bd)}({\rm total})} \right\rangle_{Y\pm 0.0075}, \qquad (35)$$

where the average is taken on the stellar trajectory over the range $Y - 0.0075 \le Y_e \le Y + 0.0075$. Thus the nuclei which make the largest contributions to $\dot{Y}_e$ will have the largest values of $\mathcal{R}$. Tables 13 to 18 list these rankings for electron capture nuclei, while Tables 19 to 24 list the rankings for beta decay nuclei. Table 12 summarizes the conditions relevant for each table. Except for $\mathcal{R}$, every other column in the tables has been evaluated at the central Y-value, in a manner similar to Tables 4 to 11. Unlike the earlier eight tables, the nuclei in Tables 13 to 24 are sorted by $\mathcal{R}$, not individual values of $\dot{Y}_e$. For the $Y_e = 0.485$, 0.470, 0.455, and 0.440 points only nuclei with $\mathcal{R} > 0.001$ have been listed. This criterion means that only nuclei which contributed, on average, more than 0.1% of $\dot{Y}_e$ throughout the range are listed. As the trajectory becomes more neutron rich, many more nuclei contribute to $\dot{Y}_e$. Thus, the criterion is raised to $\mathcal{R} > 0.01$ for the $Y_e = 0.425$ and 0.410. If one wishes to know on which nuclei to perform more detailed studies, the top of each list provides which nuclei to start with for a given part of the trajectory. The nuclei ^{52}V, ^{52,54}Cr, ^{56,58}Fe, and ^{60}Co appear in Tables 13 to 18 with two entries for $\mathcal{R}$. These nuclei have been severely underpredicted in the effective treatment and so their ranking obtained just with FFN rates has been used to place them in the tables. The entries in the $\mathcal{R}$ column in parentheses list the values for $\mathcal{R}$ obtained using the effective rates. Similar cases occur for the beta-decay tables for the nuclei ^{52}Ti, ^{54,56}Cr, ^{57}Mn, and ^{58}Fe.

In order to obtain an overview of which nuclei are important along the whole stellar trajectory, we have also computed a ranking parameter for $0.40 \le Y_e \le 0.50$:

$$\mathcal{R} = \left\langle \frac{\dot{Y}_e^{\rm ec(bd)}(k)}{\dot{Y}_e^{\rm ec(bd)}({\rm total})} \right\rangle_{0.40<Y<0.50}. \qquad (36)$$

Again a lower limit of $\mathcal{R} \ge 0.001$ was chosen. Tables 25 and 26 list these overall rankings for electron capture and beta-decay,

TABLE 12

SUMMARY OF CONDITIONS USED FOR RANKING TABLES

ρ (g cm^{-3})	T_9	Y_e	Capture Table	Decay Table
4.32E+07	3.26	0.4850 ± 0.0075	13	19
5.86E+07	3.40	0.4700 ± 0.0075	14	20
1.07E+08	3.65	0.4550 ± 0.0075	15	21
3.30E+08	4.24	0.4400 ± 0.0075	16	22
2.20E+09	5.39	0.4250 ± 0.0075	17	23
4.01E+10	7.33	0.4100 ± 0.0075	18	24

TABLE 13

LIST OF NUCLEI

(ELECTRON CAPTURE: $\rho = 4.32E+07$, $T_9 = 3.26E+00$, $Y_e = 0.4850 \pm 0.0075$)

^AZ	X_k	λ_k^{ec} (s^{-1})	$\lvert \dot{Y}_e^{ec}(k) \rvert$ (s^{-1})	$\mathscr{R}$	Ratio	$\mathscr{F}$	Fraction GT
^{55}Co	5.15E−02	5.13E−02	4.80E−05	5.01E−01	6.09E−01	1	7.33E−01
^{56}Ni	1.37E−01	8.55E−03	2.09E−05	2.54E−01	1.15E+00	2	1.82E−01
^{54}Fe	5.27E−01	1.78E−04	1.74E−06	5.88E−02	1.16E+00	4	8.79E−04
^{57}Ni	2.25E−02	1.34E−02	5.30E−06	5.38E−02	2.12E+00	3	3.07E−02
^{58}Ni	2.50E−01	3.86E−04	1.66E−06	4.31E−02	1.93E+00	6	1.81E−03
^{56}Co	1.37E−03	3.42E−02	8.34E−07	2.62E−02	8.14E−01	5	3.71E−01
^{57}Co	2.69E−03	2.36E−03	1.11E−07	2.56E−02	2.09E+00	10	1.14E−02
^{55}Fe	2.96E−03	1.06E−03	5.72E−08	1.56E−02	1.28E+00	11	1.63E−05
^{59}Ni	5.13E−04	3.06E−03	2.66E−08	5.20E−03	1.10E+00	13	1.67E−04
^{53}Mn	4.86E−04	1.68E−03	1.54E−08	5.18E−03	2.13E+00	14	4.47E−03
^{53}Fe	1.53E−03	1.50E−02	4.34E−07	4.68E−03	5.31E−01	7	1.72E−08
^{61}Cu	5.73E−06	1.34E−01	1.26E−08	2.28E−03	...	...	9.43E−01
^{59}Cu	3.73E−05	3.68E−01	2.33E−07	2.26E−03	3.69E+00	9	9.32E−01
^{52}Fe	9.92E−04	7.56E−03	1.44E−07	1.59E−03	8.92E−01	8	8.08E−08

$\dot{Y}_e^{tot} = -7.95E{-}05\ s^{-1}$, $\dot{Y}_e^{tot}(FFN) = -1.04E{-}04\ s^{-1}$

NOTES.—List of nuclei sorted in order of ranking parameter $\mathscr{R}$, as defined in eq. (35). The Y_e range over which $\mathscr{R}$ has been computed is given above the table. All other columns are as defined in Table 4, evaluated at the temperature, density, and central Y_e given above the table.

respectively. It can be seen that the top nuclei here are the same nuclei which appeared as top nuclei in Figures 10 and 11 and at the head of the lists for parts of the trajectory. The nuclei marked with asterisks were severely underpredicted by the effective rates and so their ranking was computed using their FFN rates. These overall rankings are the ultimate objective of this study. These tables allow future, more detailed, studies of individual nuclei to be prioritized.

We conclude our discussion of the stellar trajectory by noting a feature of the total electron capture and beta-decay $\dot{Y}_e$ profiles which had not been expected. Figure 14 compares the total $\dot{Y}_e$ curves, as shown separately in Figures 10 and 11. It can be seen that, early in the trajectory (at large Y_e), $|\dot{Y}_e|$ due to electron capture is dominant. However, as Y_e drops, the beta-decay $\dot{Y}_e$ becomes stronger and stronger. Near $Y_e \sim 0.455$, the net $\dot{Y}_e$ tends to zero as the electron capture and beta-decay contributions balance one another. This effect is surprising in view of the standard belief that electron capture reactions dominate the evolution of Y_e after silicon burning.

The strength of the beta-decay contributions to $\dot{Y}_e$ are fairly robust. It is not the result of a single nucleus decaying. As Table 21 shows, many nuclei are contributing to $\dot{Y}_e$. Figure 13 shows that the decays are able to rival the electron captures because the decays are occuring through thermal excitation of the GT back resonance. Thus this behavior is different from what was discussed by Aufderheide et al. (1990). They had suggested that several $A > 60$ nuclei with large beta-decay Q-values could cool the core. Such a scenario is prevented for two reasons. Firstly, as has been seen here, the decays are dominated by back resonances and not simply by which nucleus has a large Q-value. Secondly, the nuclei mentioned by Aufderheide et al. (1990) are not very abundant in the core until just before collapse, by which time the dynamical timescale is becoming shorter than the weak interaction timescale. The effects seen here have a larger effect because they occur much earlier in the evolution and many nuclei contribute.

Because the full rates indicate that the total $\dot{Y}_e$ tends to zero as the trajectory passes through $Y_e \sim 0.455$, the trajectory is not consistent below this value of Y_e. From this point onward, inclusion of the FFN beta-decay rates could drastically affect Y_e (and temperature because of enhanced neutrino emission) along the trajectory. It is beyond the scope of this paper to explore these matters. In a separate paper (Aufderheide et al. 1994) these questions are examined using a one zone mode and only FFN rates. In future work, a more detailed study of this problem will be made.

6. CONCLUSIONS

In this paper we have developed a set of effective electron capture and beta-decay rates and folded them into an NSE distribution of elements in order to determine which nuclei have the largest effect on Y_e for conditions after silicon core burning. With this tool we have been able to rank nuclei in order of how strongly they affect Y_e. These rankings are given for several points after silicon core burning in Tables 13 to 24. Tables 25 and 26 provide an overall ranking for all conditions which follow silicon core burning. These tables are the most important result of this paper.

In the process of developing and analyzing these effective rates, several insights have been gained. Firstly, the relative importance of the GT resonance can be stated in a more quantitative fashion. For electron captures, the GT resonance provides roughly 20% to 60% of the total change in Y_e. Figure 13 demonstrates this trend. Thus low-lying transitions do provide a sizeable part of the change in Y_e. The cases where the effective electron capture rates made the worst underestimates were cases dominated by low-lying transitions. Surprisingly, the beta-decays are even more strongly dominated by the GT (back) resonance. It can be seen that 30% to 100% of the changes in Y_e are due to decays from the thermally populated back resonance. Again the low-lying structure of these nuclei is

TABLE 14

LIST OF NUCLEI

(ELECTRON CAPTURE: ρ = 5.86E+07, T_9 = 3.40E+00, Y_e = 0.4700 ± 0.0075)

^AZ	X_k	λ_k^{ec} (s^{-1})	$\lvert \dot{Y}_e^{ec}(k) \rvert$ (s^{-1})	$\mathcal{R}$	Ratio	$\mathcal{F}$	Fraction GT
^{57}Co	3.55E−02	3.43E−03	2.14E−06	2.46E−01	1.82E+00	3	1.91E−02
^{55}Fe	5.20E−02	1.61E−03	1.52E−06	1.92E−01	1.03E+00	1	3.62E−05
^{54}Fe	2.11E−01	3.10E−04	1.21E−06	1.26E−01	1.05E+00	4	1.54E−03
^{55}Co	5.35E−04	7.99E−02	7.77E−07	1.18E−01	5.86E−01	2	7.68E−01
^{53}Mn	1.30E−02	2.46E−03	6.04E−07	8.79E−02	1.89E+00	8	7.72E−03
^{58}Ni	5.44E−02	6.34E−04	5.95E−07	6.53E−02	1.70E+00	7	3.19E−03
^{56}Co	5.56E−04	5.14E−02	5.11E−07	5.29E−02	7.44E−01	5	4.38E−01
^{59}Ni	5.13E−03	4.37E−03	3.80E−07	4.07E−02	1.01E+00	6	3.43E−04
^{61}Cu	5.00E−05	2.02E−01	1.65E−07	1.70E−02	...	...	9.47E−01
^{54}Mn	2.16E−04	5.13E−03	2.05E−08	1.69E−02	3.64E+00	16	2.92E−04
^{56}Fe	5.05E−01	6.97E−08	6.29E−10	1.20E−02 (4.34E−04)	4.45E−02	11	5.84−04
^{58}Co	1.31E−04	1.04E−02	2.34E−08	1.01E−02	2.82E+00	14	4.77E−03
^{57}Ni	1.71E−04	1.85E−02	5.57E−08	9.27E−03	1.87E+00	9	4.82E−02
^{60}Ni	8.90E−02	1.25E−06	1.85E−09	6.13E−03 (6.91E−04)	1.36E−01	12	1.95E−01
^{51}Cr	3.57E−04	2.81E−03	1.97E−08	3.50E−03	2.14E+00	13	1.11E−11
^{59}Co	5.59E−04	4.57E−05	4.33E−10	2.58E−03	1.18E+00	22	2.15E−01
^{62}Cu	7.23E−07	8.06E−01	9.40E−09	2.57E−03	...	...	9.70E−01
^{56}Ni	2.72E−05	1.28E−02	6.23E−09	1.89E−03	9.84E−01	15	2.47E−01
^{53}Fe	2.52E−05	2.04E−02	9.70E−09	1.39E−03	5.21E−01	10	5.14E−08

$\dot{Y}_e^{tot}$ = −8.07E−06 s^{-1}, $\dot{Y}_e^{tot}$(FFN) = −6.98E−06 s^{-1}

NOTE.—Columns are as explained in Table 13.

TABLE 15

LIST OF NUCLEI

(ELECTRON CAPTURE: ρ = 1.07E+08, T_9 = 3.65E+00, Y_e = 0.4550 ± 0.0075)

^AZ	X_k	λ_k^{ec} (s^{-1})	$\lvert \dot{Y}_e^{ec}(k) \rvert$ (s^{-1})	$\mathcal{R}$	Ratio	$\mathcal{F}$	Fraction GT
^{54}Mn	4.75E−04	1.06E−02	9.33E−08	1.88E−01	2.34E+00	4	1.03E−03
^{59}Co	1.75E−02	2.09E−04	6.21E−08	1.51E−01	1.01E+00	2	3.05E−01
^{55}Fe	6.68E−04	3.80E−03	4.61E−08	1.26E−01	6.51E−01	1	1.45E−04
^{56}Fe	2.89E−01	4.68E−07	2.41E−09	1.16E−01 (4.92E−03)	4.52E−02	3	1.41E−03
^{60}Co	3.45E−04	4.07E−03	2.34E−08	1.07E−01	7.97E−01	5	4.86E−01
^{57}Co	2.53E−04	7.65E−03	3.39E−08	1.01E−01	1.36E+00	7	4.82E−02
^{53}Mn	3.74E−04	5.57E−03	3.92E−08	9.72E−02	1.48E+00	6	2.05E−02
^{58}Co	7.81E−05	2.06E−02	2.78E−08	5.71E−02	2.25E+00	9	1.38E−02
^{61}Ni	2.55E−03	3.92E−04	1.64E−08	3.69E−02	...	...	3.14E−01
^{64}Cu	5.28E−06	1.18E−01	9.74E−09	3.10E−02	...	...	8.74E−01
^{63}Cu	9.55E−05	5.92E−03	8.97E−09	1.89E−02	...	...	5.18E−01
^{55}Mn	3.21E−02	9.23E−06	5.38E−09	1.69E−02	1.14E+00	12	1.40E−03
^{52}Cr	8.06E−02	2.01E−07	3.12E−10	1.48E−02 (7.13E−04)	4.95E−02	10	7.90E−04
^{59}Ni	2.06E−05	9.23E−03	3.22E−09	1.05E−02	8.62E−01	13	1.23E−03
^{62}Cu	1.62E−07	1.61E+00	4.21E−09	8.93E−03	...	...	9.71E−01
^{51}Cr	2.57E−05	6.14E−03	3.09E−09	6.96E−03	1.92E+00	15	1.35E−10
^{57}Fe	1.56E−02	7.47E−06	2.04E−09	5.66E−03	4.05E−01	11	1.60E−05
^{51}V	4.08E−03	1.24E−05	9.89E−10	4.57E−03	2.79E+00	17	7.63E−04
^{56}Mn	2.77E−04	1.21E−04	5.97E−10	4.35E−03	6.34E+00	20	1.80E−05
^{60}Ni	1.51E−02	7.64E−06	1.92E−09	3.93E−03	1.44E−01	8	2.78E−01
^{61}Cu	1.42E−07	4.73E−01	1.10E−09	3.52E−03	...	...	9.56E−01
^{54}Fe	3.87E−05	9.50E−04	6.80E−10	3.21E−03	9.10E−01	16	4.05E−03
^{53}Cr	1.86E−02	9.13E−07	3.20E−10	1.28E−03	1.47E−01	14	6.64E−06

$\dot{Y}_e^{tot}$ = −3.90E−07 s^{-1}, $\dot{Y}_e^{tot}$(FFN) = −3.58E−07 s^{-1}

NOTE.—Columns are as explained in Table 13.

TABLE 16

LIST OF NUCLEI
(ELECTRON CAPTURE: ρ = 3.30E+08, T_9 = 4.24E+00, Y_e = 0.4400 ± 0.0075)

^AZ	X_k	λ_k^{ec} (s^{-1})	$\lvert\dot{Y}_e^{ec}(k)\rvert$ (s^{-1})	$\mathcal{R}$	Ratio	$\mathcal{F}$	Fraction GT
^{60}Co	3.26E−04	6.09E−02	3.31E−07	5.13E−01	5.66E−01	1	7.70E−01
^{59}Co	5.16E−04	5.07E−03	4.43E−08	1.00E−01	5.50E−01	2	5.50E−01
^{66}Cu	9.05E−05	2.68E−02	3.67E−08	6.61E−02	...	...	4.37E−01
^{56}Mn	1.12E−03	1.96E−03	3.92E−08	5.76E−02	4.73E+00	6	2.16E−04
^{64}Cu	1.97E−06	7.82E−01	2.41E−08	4.42E−02	...	...	9.20E−01
^{55}Mn	3.62E−03	2.64E−04	1.74E−08	3.04E−02	1.04E+00	3	7.34E−03
^{51}V	2.68E−03	3.31E−04	1.74E−08	2.79E−02	2.62E+00	8	4.10E−03
^{54}Mn	5.72E−06	4.71E−02	4.99E−09	2.33E−02	6.74E−01	7	1.25E−02
^{52}V	6.76E−04	9.40E−04	1.22E−08	2.24E−02	4.43E+00	10	8.04E−05
^{61}Ni	4.39E−05	8.38E−03	6.03E−09	1.60E−02	...	...	5.78E−01
^{65}Cu	5.52E−04	1.10E−03	9.32E−09	1.46E−02	...	...	2.70E−01
^{62}Co	4.31E−04	4.68E−04	3.25E−09	1.13E−02	...	...	2.99E−01
^{61}Co	1.40E−02	1.67E−05	3.82E−09	8.44E−03	...	...	3.19E−01
^{57}Fe	8.47E−04	2.21E−04	3.29E−09	6.37E−03	2.88E−01	5	1.67E−04
^{68}Cu	6.03E−05	9.97E−04	8.84E−10	6.24E−03	...	...	5.11E−02
^{67}Cu	2.69E−03	3.50E−05	1.41E−09	5.76E−03	...	...	7.51E−02
^{49}Ti	1.85E−04	8.68E−04	3.27E−09	5.37E−03	4.95E+00	13	1.66E−10
^{63}Cu	1.26E−06	8.42E−02	1.69E−09	5.33E−03	...	...	7.90E−01
^{53}Cr	4.39E−03	3.77E−05	3.12E−09	5.20E−03	1.92E−01	4	7.22E−05
^{52}Cr	7.25E−04	1.06E−05	1.47E−10	4.67E−03 (3.52E−04)	7.21E−02	12	4.18−03
^{63}Ni	3.79E−03	3.41E−05	2.05E−09	3.89E−03	...	...	2.92E−01
^{58}Fe	1.52E−01	5.45E−08	1.43E−10	3.45E−03 (2.73E−04)	5.71E−02	11	3.40E−01
^{58}Co	2.81E−07	9.07E−02	4.39E−10	3.20E−03	1.10E+00	16	1.08E−01
^{53}Mn	2.66E−07	3.19E−02	1.60E−10	1.85E−03	7.51E−01	19	1.34E−01
^{60}Ni	9.37E−06	3.34E−04	5.21E−11	1.56E−03 (2.93E−04)	1.77E−01	18	4.79E−01
^{55}Fe	1.94E−07	2.13E−02	7.48E−11	1.35E−03	2.08E−01	17	2.27E−03
^{57}Mn	8.60E−03	2.19E−06	3.31E−10	1.19E−03	1.95E+01	25	3.20E−01
^{54}Cr	2.02E−01	5.65E−09	2.12E−11	1.09E−03 (5.07E−05)	3.71E−02	14	3.28E−03
^{67}Zn	2.91E−06	1.62E−02	7.05E−10	1.07E−03	...	...	3.49E−01
^{59}Fe	2.44E−02	8.67E−07	3.59E−10	1.05E−03	7.25E−01	15	3.14E−01

$\dot{Y}_e^{tot}$ = −5.73E−07 s^{-1}, $\dot{Y}_e^{tot}$(FFN) = −7.46E−07 s^{-1}

NOTE.—Columns are as explained in Table 13.

important, but for beta decays, because of the parent and daughter partition functions, which can be sensitive to low-lying states above the ground state.

Another major insight obtained in this work was the great strength of the beta-decay reactions. Because of the strength of the back resonance, the decays are able to compete with, and even balance, the changes in Y_e caused by electron capture. The full ramifications of this insight will have to be explored in the future, as has been begun by Aufderheide et al. (1994).

It has been seen that some of the FFN rates used theoretically determined Q-values which resulted in values of $\dot{Y}_e$ for some nuclei which were anomalously large. This effect is the only problem which this study has been able to find with the FFN rates (setting aside the question of where to place the GT resonance, which was beyond the scope of this paper.). These problem FFN nuclei can be identified by the fact that the mass of either the parent or daughter nucleus is not given in the Table of Isotopes (Lederer & Shirley 1978). Such nuclei considered by FFN used the Seeger & Howard (1975) mass law and the mass differences seem to be too large in general. Several of these nuclei are important in the more neutron rich parts of the trajectory.

The last insight which this study has obtained is what happens as the gas becomes neutron-rich. The simplest assumption is that, as Y_e drops, $A > 60$ nuclei dominate $\dot{Y}_e$. But the cases examined here showed that such nuclei become important, but more neutron rich nuclei with $A < 60$ also contribute. Thus the distribution of important nuclei tended to increase N, the neutron number, as much as Z, the charge of the nuclei. As a result, $A > 60$ nuclei are not as important as had been expected at the early stages of this study. If one also considers the effect of the beta-decays in hindering the decrease of Y_e, the $A > 60$ nuclei are not likely to drastically change the presupernova models.

Several questions remain for future work. We have seen how theoretical mass laws can effect the rates of neutron-rich nuclei. Varying atomic masses also effect nuclear abundances. It would be useful to quantify these effects better and to know when they could be important for the supernova problem.

Another area of study will be the effect of the beta-decays on

TABLE 17

LIST OF NUCLEI

(ELECTRON CAPTURE: ρ = 2.20E+09, T_9 = 5.39E+00, Y_e = 0.4250 ± 0.0075)

^AZ	X_k	λ_k^{ec} (s^{-1})	$\lvert\dot{Y}_e^{ec}(k)\rvert$ (s^{-1})	$\mathscr{R}$	Ratio	$\mathscr{F}$	Fraction GT
^{60}Co	4.25E−05	6.83E+00	4.84E−06	1.97E−01	5.09E−01	1	9.49E−01
^{62}Co	9.49E−04	2.51E−01	3.84E−06	1.12E−01	...	...	7.45E−01
^{66}Cu	1.02E−04	1.99E+00	3.08E−06	9.54E−02	...	...	8.15E−01
^{68}Cu	1.45E−03	1.53E−01	3.27E−06	8.80E−02	...	...	3.13E−01
^{67}Cu	5.21E−03	2.64E−02	2.06E−06	5.73E−02	...	...	2.55E−01
^{58}Mn	1.88E−03	3.42E−02	1.11E−06	5.07E−02	3.25E+00	8	6.26E−01
^{61}Co	3.13E−03	2.74E−02	1.41E−06	4.48E−02	...	...	6.34E−01
^{52}V	5.61E−04	9.62E−02	1.04E−06	3.23E−02	1.69E+00	3	6.07E−03
^{56}Mn	3.09E−04	1.38E−01	7.58E−07	3.05E−02	1.96E+00	6	1.82E−02
^{57}Mn	5.92E−03	6.09E−03	6.32E−07	2.57E−02	7.47E+00	16	6.07E−01
^{58}Fe	5.15E−03	3.79E−04	3.36E−08	1.95E−02	1.29E−01	11	6.21E−01
				(1.22E−03)			
^{51}V	3.73E−04	6.58E−02	4.81E−07	1.75E−02	1.75E+00	9	8.18E−02
^{65}Cu	7.94E−05	4.03E−01	4.93E−07	1.53E−02	...	...	7.57E−01
^{59}Fe	7.52E−03	3.01E−03	3.83E−07	1.49E−02	7.23E−01	4	5.96E−01
^{57}Fe	2.66E−05	5.29E−02	2.47E−08	1.47E−02	9.19E−02	10	7.60E−03
				(1.11E−03)			
^{59}Co	1.25E−05	1.85E+00	3.94E−07	1.45E−02	5.07E−01	2	9.20E−01
^{70}Cu	9.61E−04	2.04E−02	2.80E−07	1.31E−02	...	...	0.00
^{63}Ni	5.65E−04	4.36E−02	3.91E−07	1.21E−02	...	...	6.26E−01
^{53}V	1.10E−02	1.57E−03	3.26E−07	1.21E−02	8.34E−01	5	2.57E−02
^{54}Cr	1.85E−02	3.51E−05	1.21E−08	1.19E−02	5.60E−02	13	2.89E−02
				(4.61E−04)			
^{69}Cu	1.09E−02	1.11E−03	1.75E−07	1.02E−02	...	...	0.00
^{65}Ni	3.29E−02	4.10E−04	2.07E−07	1.01E−02	...	...	2.70E−01

$\dot{Y}_e^{tot}$ = −2.84E−05 s^{-1}, $\dot{Y}_e^{tot}$(FFN) = −1.47E−05 s^{-1}

NOTE.—Columns are as explained in Table 13.

TABLE 18

LIST OF NUCLEI

(ELECTRON CAPTURE: ρ = 4.01E+10, T_9 = 7.33E+00, Y_e = 0.4100 ± 0.0075)

^AZ	X_k	λ_k^{ec} (s^{-1})	$\lvert\dot{Y}_e^{ec}(k)\rvert$ (s^{-1})	$\mathscr{R}$	Ratio	$\mathscr{F}$	Fraction GT
^{58}Mn	9.84E−04	5.36E+02	9.08E−03	7.20E−02	6.78E−01	1	9.66E−01
^{49}Sc	1.39E−02	3.13E+01	8.86E−03	5.49E−02	1.05E+00	2	6.72E−01
^{61}Fe	6.09E−03	8.45E+01	8.44E−03	3.95E−02	...	...	9.30E−01
^{57}Mn	6.87E−04	4.25E+02	5.12E−03	3.80E−02	9.89E−01	5	9.69E−01
^{62}Co	2.45E−04	7.31E+02	2.89E−03	3.66E−02	...	...	9.63E−01
^{52}V	1.21E−04	2.00E+02	4.66E−04	3.59E−02	2.35E−01	6	8.62E−01
				(3.31E−03)			
^{64}Co	2.56E−03	1.28E+02	5.12E−03	3.14E−02	...	...	8.81E−01
^{55}V	5.46E−03	4.81E+01	4.77E−03	3.04E−02	...	...	9.19E−01
^{50}Sc	1.03E−02	1.85E+01	3.80E−03	3.02E−02	...	...	3.85E−01
^{63}Co	4.78E−03	8.46E+01	6.43E−03	3.02E−02	...	...	9.17E−01
^{65}Ni	4.43E−03	7.68E+01	5.24E−03	2.96E−02	...	...	8.76E−01
^{68}Cu	1.19E−03	1.27E+02	2.22E−03	2.65E−02	...	...	7.50E−01
^{53}V	2.76E−03	9.25E+01	4.81E−03	2.57E−02	7.26E−01	3	8.73E−01
^{57}Cr	5.92E−03	3.18E+01	3.30E−03	2.35E−02	...	...	9.13E−01
^{59}Fe	5.06E−04	3.66E+02	3.14E−03	2.21E−02	4.93E−01	4	9.67E−01
^{59}Mn	3.16E−03	7.28E+01	3.90E−03	2.02E−02	...	...	9.32E−01
^{61}Co	1.80E−04	5.84E+02	1.72E−03	1.97E−02	...	...	9.69E−01
^{67}Cu	7.79E−04	1.38E+02	1.60E−03	1.92E−02	...	...	8.44E−01
^{60}Mn	1.49E−03	1.32E+02	3.28E−03	1.84E−02	...	...	9.31E−01
^{70}Cu	6.74E−03	2.16E+01	2.08E−03	1.69E−02	...	...	0.00
^{54}V	2.15E−03	5.56E+01	2.21E−03	1.53E−02	...	...	7.39E−01
^{69}Cu	9.93E−03	1.25E+01	1.80E−03	1.51E−02	...	...	0.00
^{56}Cr	6.34E−03	1.75E+01	1.98E−03	1.44E−02	...	...	9.05E−01
^{67}Ni	4.27E−02	4.46E+00	2.84E−03	1.43E−02	...	...	0.00
^{69}Ni	8.07E−02	1.50E+00	1.75E−03	1.25E−02	...	...	0.00
^{51}Ti	7.39E−03	9.39E+00	1.36E−03	1.23E−02	1.48E+00	8	3.03E−01
^{60}Fe	4.22E−03	3.50E+01	2.46E−03	1.21E−02	2.43E+00	7	9.23E−01
^{51}Sc	1.08E−02	4.16E+00	8.81E−04	1.19E−02	...	...	3.25E−01
^{81}As	1.68E−02	9.74E+00	2.03E−03	1.17E−02	...	...	0.00
^{76}Ga	6.97E−03	1.90E+01	1.74E−03	1.16E−02	...	...	0.00
^{53}Ti	1.28E−02	2.46E+00	5.96E−04	1.00E−02	...	...	6.99E−02

$\dot{Y}_e^{tot}$ = −1.38E−01 s^{-1}, $\dot{Y}_e^{tot}$(FFN) = −4.72E−02 s^{-1}

NOTE.—Columns are as explained in Table 13.

TABLE 19

LIST OF NUCLEI

(BETA-DECAY: ρ = 4.32E+07, T_9 = 3.26E+00, Y_e = 0.4850 ± 0.0075)

^AZ	X_k	λ_k^{bd} (s^{-1})	$\lvert \dot{Y}_e^{bd}(k) \rvert$ (s^{-1})	$\mathcal{R}$	Ratio	$\mathcal{F}$	Fraction GT
^{56}Co	1.37E−03	6.17E−09	1.51E−13	5.52E−01	6.09E−01	1	9.50E−01
^{54}Mn	1.74E−07	7.54E−06	2.44E−14	2.39E−01	6.49E+00	4	1.08E−01
^{58}Co	2.02E−07	3.23E−06	1.12E−14	9.06E−02	4.90E+00	5	3.50E−01
^{57}Co	2.69E−03	3.65E−10	1.72E−14	5.72E−02	3.38E−01	2	9.85E−01
^{57}Fe	7.92E−09	3.55E−06	4.94E−16	3.41E−02	1.57E+00	8	9.92E−01
^{55}Fe	2.96E−03	5.30E−11	2.85E−15	9.74E−03	3.68E−01	3	9.46E−01
^{56}Fe	8.64E−04	3.73E−11	5.76E−16	5.14E−03	3.01E−01	7	9.99E−01
^{53}Cr	1.08E−09	1.89E−06	3.83E−17	3.90E−03	2.99E−01	9	9.64E−01
^{60}Co	7.53E−14	4.03E−03	5.06E−18	2.82E−03	4.50E+00	14	1.51E−01
^{55}Mn	5.51E−09	2.76E−07	2.76E−17	2.04E−03	1.24E−02	6	9.22E−02
^{56}Mn	7.09E−15	1.16E−02	1.48E−18	1.21E−03	2.86E+00	15	8.02E−04

$\dot{Y}_e^{tot}$ = 2.08E−13 s^{-1}, $\dot{Y}_e^{tot}$(FFN) = 3.17E−13 s^{-1}

NOTE.—Columns are as explained in Table 13.

TABLE 20

LIST OF NUCLEI

(BETA-DECAY: ρ = 5.86E+07, T_9 = 3.40E+00, Y_e = 0.4700 ± 0.0075)

^AZ	X_k	λ_k^{bd} (s^{-1})	$\lvert \dot{Y}_e^{bd}(k) \rvert$ (s^{-1})	$\mathcal{R}$	Ratio	$\mathcal{F}$	Fraction GT
^{54}Mn	2.16E−04	7.46E−06	2.98E−11	3.20E−01	4.76E+00	4	1.81E−01
^{57}Fe	2.60E−04	5.54E−06	2.53E−11	2.45E−01	1.49E+00	2	9.95E−01
^{60}Co	1.02E−07	3.87E−03	6.60E−12	1.12E−01	3.56E+00	8	2.02E−01
^{56}Mn	1.98E−08	1.09E−02	3.86E−12	1.01E−01	2.86E+00	11	1.45E−03
^{58}Co	1.31E−04	3.82E−06	8.60E−12	9.60E−02	3.28E+00	5	4.82E−01
^{53}Cr	7.36E−05	3.00E−06	4.16E−12	4.60E−02	2.92E−01	3	9.75E−01
^{54}Cr	4.58E−06	1.48E−07	1.25E−14	3.15E−02 (5.23E−04)	6.75E−03	7	9.64−01
^{59}Fe	2.06E−09	3.53E−03	1.24E−13	2.21E−02	6.91E−01	14	9.66E−01
^{55}Mn	2.61E−04	3.14E−07	1.49E−12	1.50E−02	1.05E−02	1	1.72E−01
^{57}Co	3.55E−02	6.76E−10	4.21E−13	7.26E−03	3.02E−01	10	9.87E−01
^{61}Co	4.60E−09	7.08E−04	5.33E−14	6.54E−03	...	...	9.20E−01
^{56}Fe	5.05E−01	5.94E−11	5.35E−13	5.96E−03	2.64E−01	6	9.98E−01
^{59}Co	5.59E−04	4.86E−08	4.60E−13	4.34E−03	3.29E−01	9	6.71E−01
^{57}Mn	1.03E−10	2.33E−03	4.20E−15	3.79E−03 (9.65E−04)	1.52E−01	17	1.35E−04
^{56}Co	5.56E−04	8.56E−09	8.50E−14	2.96E−03	5.87E−01	15	9.51E−01
^{58}Fe	8.28E−05	5.46E−08	7.79E−14	1.81E−03	6.41E−02	12	9.96E−01
^{55}Fe	5.20E−02	6.76E−11	6.38E−14	1.18E−03	3.43E−01	13	9.30E−01
^{63}Ni	5.78E−09	1.58E−04	1.45E−14	1.16E−03	...	...	9.96E−01

$\dot{Y}_e^{tot}$ = 8.20E−11 s^{-1}, $\dot{Y}_e^{tot}$(FFN) = 1.94E−10 s^{-1}

NOTE.—Columns are as explained in Table 13.

TABLE 21

LIST OF NUCLEI

(BETA-DECAY: ρ = 1.07E+08, T_9 = 3.65E+00, Y_e = 0.4550 ± 0.0075)

^AZ	X_k	λ_k^{bd} (s^{-1})	$\lvert \dot{Y}_e^{bd}(k) \rvert$ (s^{-1})	$\mathcal{R}$	Ratio	$\mathcal{F}$	Fraction GT
^{59}Fe	9.51E−04	4.60E−03	7.40E−08	3.83E−01	7.03E−01	1	9.85E−01
^{56}Mn	2.77E−04	9.06E−03	4.49E−08	2.35E−01	3.02E+00	6	4.04E−03
^{60}Co	3.45E−04	3.43E−03	1.97E−08	1.16E−01	2.42E+00	8	3.30E−01
^{61}Co	1.07E−03	8.86E−04	1.55E−08	7.61E−02	...	...	9.59E−01
^{60}Fe	1.92E−04	1.73E−03	5.55E−09	4.16E−02	2.04E−01	4	9.99E−01
^{52}V	2.95E−05	1.37E−02	7.75E−09	3.88E−02	8.50E+00	13	1.94E−03
^{57}Fe	1.56E−02	1.02E−05	2.78E−09	2.40E−02	1.43E+00	11	9.97E−01
^{57}Mn	1.16E−04	1.70E−03	3.45E−09	1.75E−02	9.55E−02	3	6.45E−04
^{53}Cr	1.86E−02	5.81E−06	2.04E−09	1.36E−02	2.83E−01	9	9.87E−01
^{55}Cr	8.36E−05	1.47E−03	2.23E−09	1.28E−02	3.28E−01	10	1.08E−01
^{53}V	1.01E−05	6.49E−03	1.24E−09	8.35E−03	9.60E−01	12	1.60E−04
^{63}Ni	6.34E−04	1.61E−04	1.62E−09	7.66E−03	...	...	9.96E−01
^{62}Co	6.62E−07	6.68E−02	7.13E−10	6.01E−03	...	...	1.65E−01
^{58}Fe	2.85E−01	1.52E−07	7.47E−10	3.85E−03	5.80E−02	7	9.98E−01
^{54}Cr	7.30E−02	4.55E−07	6.15E−10	3.13E−03	1.18E−02	2	9.86E−01
^{58}Mn	6.72E−08	1.53E−01	1.77E−10	2.40E−03	1.13E+00	16	1.12E−01
^{55}Mn	3.21E−02	4.17E−07	2.43E−10	1.99E−03	1.06E−02	5	4.25E−01
^{51}Ti	1.18E−05	1.09E−03	2.52E−10	1.89E−03	6.66E−01	14	9.08E−02
^{65}Ni	3.42E−06	2.05E−03	1.08E−10	1.76E−03	...	...	7.72E−01
^{63}Co	2.66E−07	1.50E−02	6.34E−11	1.34E−03	...	...	3.11E−01
^{56}Cr	2.87E−06	9.73E−05	4.99E−12	1.17E−03 (5.79E−05)	3.00E−02	15	9.30E−02

$\dot{Y}_e^{tot}$ = 1.84E−07 s^{-1}, $\dot{Y}_e^{tot}$(FFN) = 2.98E−07 s^{-1}

NOTE.—Columns are as explained in Table 13.

TABLE 22

LIST OF NUCLEI

(BETA-DECAY: ρ = 3.30E+08, T_9 = 4.24E+00, Y_e = 0.4400 ± 0.0075)

^AZ	X_k	λ_k^{bd} (s^{-1})	$\lvert \dot{Y}_e^{bd}(k) \rvert$ (s^{-1})	$\mathcal{R}$	Ratio	$\mathcal{F}$	Fraction GT
^{59}Fe	2.44E−02	5.28E−03	2.19E−06	2.45E−01	9.41E−01	3	9.96E−01
^{61}Fe	1.29E−03	6.44E−02	1.36E−06	1.26E−01	...	...	8.73E−01
^{60}Fe	8.52E−02	1.00E−03	1.42E−06	1.12E−01	2.20E−01	1	9.99E−01
^{63}Co	3.34E−03	1.41E−02	7.46E−07	5.68E−02	...	...	6.36E−01
^{58}Mn	2.63E−04	1.39E−01	6.30E−07	4.96E−02	1.09E+00	8	2.55E−01
^{65}Ni	1.40E−02	2.49E−03	5.36E−07	3.66E−02	...	...	9.50E−01
^{62}Fe	3.80E−04	4.72E−02	2.90E−07	3.63E−02	...	...	9.92E−01
^{59}Mn	1.08E−04	1.58E−01	2.89E−07	3.52E−02	3.69E−01	6	7.63E−01
^{62}Co	4.31E−04	5.93E−02	4.12E−07	3.15E−02	...	...	3.63E−01
^{57}Cr	7.66E−05	1.49E−01	2.00E−07	2.93E−02	1.25E−01	4	8.43E−01
^{61}Co	1.40E−02	9.33E−04	2.14E−07	2.92E−02	...	...	9.86E−01
^{50}Sc	5.81E−05	1.79E−01	2.08E−07	2.52E−02	6.38E+00	17	1.04E−03
^{55}Cr	1.29E−02	1.06E−03	2.49E−07	2.25E−02	2.17E−01	5	6.42E−01
^{56}Mn	1.12E−03	4.58E−03	9.15E−08	2.11E−02	2.98E+00	18	3.56E−02
^{53}V	4.67E−03	2.98E−03	2.63E−07	2.05E−02	9.85E−01	12	3.56E−03
^{54}V	5.80E−05	1.90E−01	2.04E−07	1.90E−02	1.70E+00	14	2.74E−03
^{67}Ni	5.88E−04	1.20E−02	1.05E−07	1.61E−02	...	...	7.33E−01
^{52}V	6.76E−04	7.60E−03	9.88E−08	1.28E−02	8.59E+00	20	1.63E−02
^{51}Ti	9.99E−03	7.13E−04	1.40E−07	1.18E−02	4.87E−01	11	6.10E−01
^{57}Mn	8.60E−03	5.32E−04	8.02E−08	9.98E−03	2.07E−02	2	2.02E−02
^{58}Cr	5.98E−06	2.79E−01	2.88E−08	7.99E−03	6.78E−02	10	9.78E−01
^{64}Co	1.69E−05	2.05E−01	5.42E−08	7.62E−03	...	...	2.26E−01
^{66}Ni	5.24E−02	1.24E−04	9.86E−08	6.49E−03	...	...	9.94E−01
^{65}Co	9.43E−06	1.39E−01	2.02E−08	5.26E−03	...	...	3.26E−01
^{60}Co	3.26E−04	2.58E−03	1.40E−08	4.47E−03	1.26E+00	21	7.06E−01
^{52}Ti	2.47E−03	1.19E−04	5.65E−09	3.03E−02 (6.23E−04)	1.08E−02	9	3.87E−01
^{58}Fe	1.52E−01	6.39E−07	1.67E−09	2.89E−03 (3.77E−04)	7.49E−02	19	9.99E−01
^{55}V	1.27E−05	8.52E−02	1.97E−08	2.84E−03	2.16E−01	15	5.40E−04
^{56}Cr	9.82E−03	1.14E−04	2.01E−08	2.08E−03	3.11E−02	7	7.47E−01
^{68}Ni	2.11E−04	2.66E−03	8.25E−09	2.07E−03	...	...	9.60E−01
^{53}Ti	1.73E−05	3.19E−02	1.04E−08	1.74E−03	3.19E−01	16	8.07E−02
^{49}Ca	8.52E−06	4.18E−02	7.27E−09	1.73E−03	2.09E+01	28	2.12E−02
^{51}Sc	2.37E−06	1.32E−01	6.16E−09	1.50E−03	2.90E+00	25	1.48E−04
^{54}Cr	2.02E−01	2.90E−06	1.09E−08	1.28E−03	5.75E−02	13	9.97E−01
^{63}Ni	3.79E−03	8.90E−05	5.36E−09	1.19E−03	...	...	9.96E−01
^{68}Cu	6.03E−05	1.31E−02	1.16E−08	1.01E−03	...	...	2.92E−01

$\dot{Y}_e^{tot}$ = 1.01E−05 s^{-1}, $\dot{Y}_e^{tot}$(FFN) = 1.95E−05 s^{-1}

NOTE.—Columns are as explained in Table 13.

TABLE 23

LIST OF NUCLEI

(BETA-DECAY: ρ = 2.20E+09, T_9 = 5.39E+00, Y_e = 0.4250 ± 0.0075)

^AZ	X_k	λ_k^{bd} (s^{-1})	$\lvert\dot{Y}_e^{bd}(k)\rvert$ (s^{-1})	$\mathcal{R}$	Ratio	$\mathcal{F}$	Fraction GT
^{61}Fe	1.47E−02	3.54E−02	8.50E−06	1.19E−01	...	...	9.91E−01
^{57}Cr	4.37E−03	1.20E−01	9.17E−06	1.04E−01	7.88E−02	2	9.86E−01
^{59}Mn	3.38E−03	1.39E−01	7.93E−06	9.51E−02	1.94E−01	3	9.73E−01
^{50}Sc	4.66E−03	5.54E−02	5.16E−06	6.24E−02	8.40E+00	14	2.09E−02
^{65}Co	3.50E−03	8.17E−02	4.40E−06	6.01E−02	...	...	7.90E−01
^{58}Cr	1.78E−03	1.64E−01	5.03E−06	5.05E−02	3.82E−02	1	9.99E−01
^{62}Fe	1.62E−02	9.63E−03	2.51E−06	4.13E−02	...	...	9.98E−01
^{64}Co	1.44E−03	1.14E−01	2.56E−06	3.73E−02	...	...	6.10E−01
^{58}Mn	1.88E−03	7.25E−02	2.35E−06	3.56E−02	1.01E+00	8	6.96E−01
^{67}Ni	4.74E−02	4.02E−03	2.85E−06	3.37E−02	...	...	9.77E−01
^{63}Fe	2.86E−04	3.54E−01	1.61E−06	3.33E−02	...	...	8.84E−01
^{61}Mn	1.73E−04	3.78E−01	1.07E−06	2.89E−02	...	...	8.32E−01
^{52}Ti	3.11E−02	4.49E−04	2.69E−07	2.84E−02	3.27E−02	4	9.90E−01
				(3.53E−03)			
^{63}Co	1.89E−02	5.27E−03	1.58E−06	2.75E−02	...	...	9.67E−01
^{54}V	1.66E−03	6.08E−02	1.87E−06	2.54E−02	2.66E+00	13	5.11E−02
^{60}Mn	2.17E−04	3.38E−01	1.22E−06	2.53E−02	5.57E−01	9	4.15E−01
^{49}Ca	6.00E−03	9.31E−03	1.14E−06	2.45E−02	6.77E−01	10	4.97E−01
^{66}Co	2.06E−04	3.24E−01	1.01E−06	2.31E−02	...	...	0.00
^{53}Ti	3.86E−03	1.47E−02	1.07E−06	2.28E−02	4.25E−01	7	8.26E−01
^{56}Cr	3.21E−02	6.91E−04	3.96E−07	1.18E−02	1.26E−01	6	9.97E−01
				(4.73E−03)			
^{51}Sc	1.51E−03	3.44E−02	1.02E−06	1.16E−02	2.40E+00	15	1.06E−02

$\dot{Y}_e^{tot}$ = 6.87E−05 s^{-1}, $\dot{Y}_e^{tot}$(FFN) = 3.17E−04 s^{-1}

NOTE.—Columns are as explained in Table 13.

TABLE 24

LIST OF NUCLEI

(BETA-DECAY: ρ = 4.01E+10, T_9 = 7.33E+00, Y_e = 0.4100 ± 0.0075)

^AZ	X_k	λ_k^{bd} (s^{-1})	$\lvert\dot{Y}_e^{bd}(k)\rvert$ (s^{-1})	$\mathcal{R}$	Ratio	$\mathcal{F}$	Fraction GT
^{53}Sc	5.70E−04	7.94E−04	8.53E−09	9.14E−02	...	...	9.70E−01
^{52}Sc	1.24E−03	5.78E−04	1.38E−08	8.36E−02	...	...	8.83E−01
^{56}V	5.16E−04	1.02E−03	9.43E−09	6.32E−02	...	...	9.78E−01
^{62}Mn	1.53E−04	4.04E−03	9.95E−09	5.89E−02	...	...	9.25E−01
^{60}Mn	1.49E−03	2.26E−04	5.62E−09	5.14E−02	1.94E−02	1	9.45E−01
^{57}V	3.77E−04	9.28E−04	6.13E−09	5.00E−02	...	...	9.83E−01
^{61}Mn	2.65E−03	9.38E−05	4.08E−09	4.83E−02	...	...	9.81E−01
^{55}Ti	4.97E−04	4.87E−04	4.41E−09	4.09E−02	...	...	9.89E−01
^{49}Ca	3.88E−02	4.46E−06	3.53E−09	3.95E−02	6.07E−02	5	9.72E−01
^{68}Co	8.07E−04	6.98E−04	8.28E−09	3.84E−02	...	...	0.00
^{51}Ca	3.13E−04	7.42E−04	4.56E−09	3.78E−02	...	...	9.85E−01
^{51}Sc	1.08E−02	3.06E−05	6.49E−09	3.69E−02	8.63E−02	3	9.71E−01
^{63}Fe	2.42E−03	5.89E−05	2.27E−09	3.18E−02	...	...	9.84E−01
^{50}Ca	7.68E−03	2.23E−05	3.43E−09	2.80E−02	...	...	9.97E−01
^{59}Cr	8.58E−04	1.76E−04	2.56E−09	2.59E−02	...	...	9.84E−01
^{66}Co	4.42E−03	3.43E−05	2.29E−09	2.47E−02	...	...	0.00
^{53}Ti	1.28E−02	7.70E−06	1.86E−09	2.45E−02	5.65E−02	7	9.91E−01
^{65}Co	9.86E−03	6.77E−06	1.03E−09	1.92E−02	...	...	9.46E−01
^{55}V	5.46E−03	2.89E−05	2.87E−09	1.83E−02	1.54E−02	2	9.87E−01
^{50}Sc	1.03E−02	8.88E−06	1.83E−09	1.67E−02	1.12E−01	9	8.16E−01
^{54}Ti	4.17E−03	2.32E−05	1.79E−09	1.64E−02	...	...	9.99E−01
^{64}Co	2.56E−03	2.30E−05	9.22E−10	1.61E−02	...	...	9.55E−01
^{84}As	1.40E−03	1.35E−04	2.25E−09	1.14E−02	...	...	0.00

$\dot{Y}_e^{tot}$ = 1.21E−07 s^{-1}, $\dot{Y}_e^{tot}$(FFN) = 8.38E−07 s^{-1}

NOTE.—Columns are as explained in Table 13.

TABLE 25

ELECTRON CAPTURE NUCLEI

^AZ	$\mathscr{R}$	^AZ	$\mathscr{R}$
^{60}Co	1.21E−01	^{54}V	3.64E−03
^{55}Co	1.10E−01	^{54}Cr*	3.55E−03
^{56}Ni	9.70E−02	^{60}Mn	3.52E−03
^{57}Co	5.52E−02	^{61}Cu	3.41E−03
^{55}Fe	4.93E−02	^{48}Sc	3.33E−03
^{59}Co	3.96E−02	^{52}Cr*	3.09E−03
^{54}Mn	3.40E−02	^{63}Ni	2.86E−03
^{53}Mn	2.82E−02	^{51}Sc	2.82E−03
^{54}Fe	2.80E−02	^{56}Cr	2.77E−03
^{66}Cu	2.47E−02	^{53}Ti	2.66E−03
^{62}Co	2.37E−02	^{51}Ti	2.62E−03
^{56}Fe*	2.10E−02	^{69}Ni	2.61E−03
^{58}Mn	1.85E−02	^{67}Ni	2.55E−03
^{68}Cu	1.81E−02	^{76}Ga	2.37E−03
^{58}Ni	1.62E−02	^{60}Fe	2.18E−03
^{56}Mn	1.40E−02	^{81}As	2.17E−03
^{49}Sc	1.29E−02	^{52}Ti	2.02E−03
^{52}V*	1.25E−02	^{77}Ga	2.00E−03
^{67}Cu	1.22E−02	^{57}Fe	1.94E−03
^{56}Co	1.19E−02	^{62}Fe	1.87E−03
^{57}Ni	1.18E−02	^{79}Ge	1.83E−03
^{64}Cu	1.15E−02	^{83}Se	1.77E−03
^{61}Co	1.08E−02	^{62}Cu	1.74E−03
^{58}Co	1.04E−02	^{78}Ga	1.67E−03
^{57}Mn	9.68E−03	^{80}As	1.63E−03
^{59}Ni	8.39E−03	^{51}Cr	1.59E−03
^{55}Mn	8.20E−03	^{49}Ti	1.59E−03
^{61}Ni	8.12E−03	^{53}Cr	1.50E−03
^{51}V	7.65E−03	^{55}Cr	1.49E−03
^{61}Fe	7.09E−03	^{71}Cu	1.45E−03
^{50}Sc	6.73E−03	^{80}Ge	1.44E−03
^{64}Co	6.30E−03	^{56}V	1.42E−03
^{65}Ni	6.16E−03	^{61}Mn	1.28E−03
^{53}V	6.07E−03	^{58}Cr	1.27E−03
^{55}V	6.03E−03	^{77}Ge	1.26E−03
^{59}Fe	5.67E−03	^{75}Zn	1.24E−03
^{60}Ni*	5.60E−03	^{74}Ga	1.21E−03
^{58}Fe*	5.53E−03	^{83}As	1.19E−03
^{63}Co	5.45E−03	^{64}Ni	1.19E−03
^{57}Cr	4.70E−03	^{72}Cu	1.19E−03
^{65}Cu	4.65E−03	^{54}Ti	1.17E−03
^{70}Cu	4.55E−03	^{82}As	1.16E−03
^{69}Cu	3.76E−03	^{68}Ni	1.11E−03
^{59}Mn	3.76E−03	^{50}V	1.06E−03
^{63}Cu	3.72E−03	^{53}Fe	1.05E−03

NOTES.—The 90 top electron capture nuclei averaged throughout the stellar trajectory for $0.40 \leq Y_e \leq 0.5$ are listed. The ranking parameter $\mathscr{R}$ is as defined in eq. (36). The most important nucleus is in the upper left corner, while the 90th most important nucleus is in the lower right corner. The nuclei marked with an asterisk (*) were underpredicted by the effective rates and so the ranking with FFN rates has been used instead.

TABLE 26

BETA-DECAY NUCLEI

^AZ	$\mathscr{R}$	^AZ	$\mathscr{R}$
^{56}Co	1.58E−01	^{65}Ni	6.84E−03
^{59}Fe	9.63E−02	^{62}Co	6.76E−03
^{54}Mn	8.34E−02	^{68}Co	6.41E−03
^{56}Mn	5.20E−02	^{55}Cr	6.18E−03
^{57}Fe	4.57E−02	^{56}Cr*	6.01E−03
^{57}Mn*	4.33E−02	^{50}Ca	5.53E−03
^{61}Fe	3.68E−02	^{59}Cr	5.42E−03
^{60}Co	3.43E−02	^{55}V	4.72E−03
^{54}Cr*	2.98E−02	^{53}V	4.57E−03
^{58}Co	2.79E−02	^{54}Ti	3.25E−03
^{60}Fe	2.35E−02	^{51}Ti	3.21E−03
^{57}Cr	2.13E−02	^{55}Mn	2.86E−03
^{59}Mn	2.07E−02	^{56}Fe	1.65E−03
^{53}Sc	1.98E−02	^{60}Cr	1.65E−03
^{61}Co	1.65E−02	^{80}Ga	1.62E−03
^{52}Sc	1.62E−02	^{63}Ni	1.47E−03
^{50}Sc	1.57E−02	^{63}Mn	1.43E−03
^{58}Mn	1.36E−02	^{54}Sc	1.33E−03
^{63}Co	1.28E−02	^{66}Ni	1.28E−03
^{65}Co	1.25E−02	^{58}V	1.24E−03
^{60}Mn	1.19E−02	^{69}Ni	1.18E−03
^{61}Mn	1.18E−02	^{74}Cu	1.17E−03
^{56}V	1.17E−02	^{68}Ni	1.05E−03
^{62}Fe	1.15E−02	^{70}Co	8.35E−04
^{53}Cr	9.54E−03	^{78}Ga	8.19E−04
^{52}Ti*	9.05E−03	^{59}Co	8.06E−04
^{64}Co	8.98E−03	^{56}Ti	7.18E−04
^{52}V	8.55E−03	^{69}Co	4.83E−04
^{51}Sc	8.50E−03	^{76}Cu	4.37E−04
^{55}Ti	8.19E−03	^{50}V	3.99E−04
^{51}Ca	8.19E−03	^{82}As	3.45E−04
^{58}Fe*	8.10E−03	^{72}Cu	3.08E−04
^{54}V	7.91E−03	^{68}Cu	2.90E−04
^{67}Ni	7.54E−03	^{71}Ni	2.73E−04
^{53}Ti	7.30E−03	^{86}Br	2.71E−04
^{66}Co	6.92E−03		

NOTES.—The 71 top beta-decay nuclei averaged throughout the stellar trajectory for $0.40 \leq Y_e \leq 0.5$ are listed. The ranking parameter $\mathscr{R}$ is as defined in eq. (36). The most important nucleus is in the upper left corner, while the 71st most important nucleus is in the lower right corner. The nuclei marked with an asterisk (*) were underpredicted by the effective rates and so the ranking with FFN rates has been used instead.

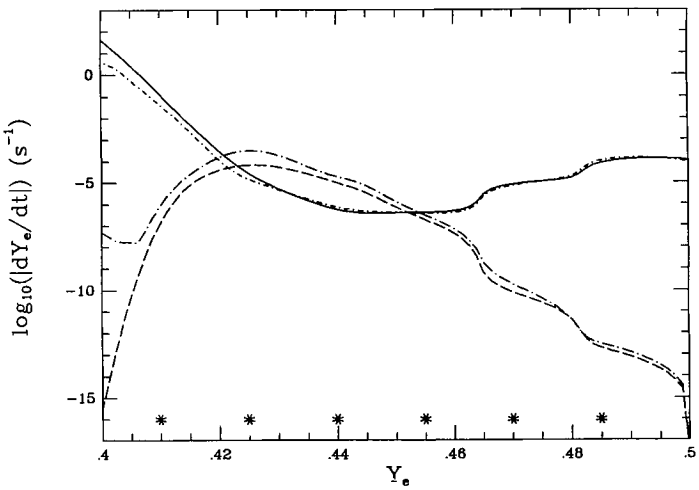

FIG. 14.—Comparison of the total $\dot{Y}_e$ due to electron capture and beta-decay. The solid (*dot-short dashed*) curve denotes the total $\dot{Y}_e$ due to electron capture using the effective (FFN) rates. The long dashed (*dot-long dashed*) curve denotes the total $\dot{Y}_e$ due to beta-decay using the effective (FFN) rates. The asterisks (*) show where along the trajectory a ranking of important nuclei has been made.

presupernova evolution and core collapse. As noted in Aufderheide et al. (1994) the decays have significant cooling ability and could affect core collapse. The final answers will come from using the most accurately known rates in a full stellar evolution code, but some useful information can be gained from one-zone models (Fuller 1982). We hope to do some of this work.

In this study we have limited ourselves to the evolution before core collapse. Continuing into collapse requires calculating high-density corrections to the theoretical mass law, and larger networks. We would like to extend this study into that regime, in order to compare with the mean-nucleus equation of state (Epstein & Arnett 1975; Bethe et al. 1979). Burrows & Lattimer (1984) studied the thermodynamic consistency of this approach. A natural extension of our study would be to see how accurately $\dot{Y}_e$ is calculated with the mean nucleus approach. At some point in the collapse, free protons dominate $\dot{Y}_e$, but the purpose of our study would be to examine the transition from the presupernova regime to the collapse, free proton dominated, regime. Fuller (1982), Zaringhalam (1983), and Cooperstein & Wambach (1984) have performed some parts of such a study.

The last area of future work is the largest: providing an update of the FFN rates. Using the new experimental information about GT resonances obtained from (n, p) reactions, it is now possible to more accurately place GT resonances for calculating electron capture and beta-decay rates. This study has helped to show which nuclei to attack first.

We thank G. M. Fuller for many valuable conversations and for providing details of how the FFN rates were constructed. We thank the Institute for Nuclear Theory at the University of Washington for its hospitality and partial support during the early stages of this work. Work at LLNL was performed under the auspices of the US Department of Energy under contract W-7405-ENG-48 and DOE nuclear theory grant SF-ENG-48. This work was also supported by grants NSF AST 8813649, NSF AST 9115367, and NASA grant NAG 5-1578.

REFERENCES

Alford, W. P., et al. 1992, Bull. Am. Phys. Soc., 37, 1298
Aufderheide, M. B. 1991, Nucl. Phys., A526, 161
Aufderheide, M. B., Bloom, S. D., Resler, D. A., & Mathews, G. J. 1993a, Phys. Rev. C, in press
———. 1993b, Phys. Rev. C, submitted
Aufderheide, M. B., Brown, G. E., Kuo, T. T. S., Stout, D. B., & Vogel, P. 1990, ApJ, 362, 241
Aufderheide, M. B., Fushiki, I., Fuller, G. M., & Weaver, T. A. 1994, ApJ, in press
Bethe, H. A., Brown, G. E., Applegate, J., & Lattimer, J. M. 1979, Nucl. Phys., A324, 487
Burrows, A. S., & Lattimer, J. M. 1984, ApJ, 285, 294
Clifford, F. E., & Tayler, R. J. 1965, MmRAS, 69, Pt. 2, 21
Comay, E., Kelson, I., & Zidon, A. 1988, ADNDT, 39, 235
Cooperstein, J., & Wambach, J. 1984, Nucl. Phys., A420, 591
Cowan, J. J., Thielemann, F.-K., & Truran, J. W. 1991, Phys. Rep., 208, 267
El Eid, M. F., & Hillebrandt, W. 1980, A&AS, 42, 215
Egawa, Y., Yokoi, K., & Yamada, M. 1975, Prog. Theor. Phys., 54, 1339
Epstein, R. I., & Arnett, W. D., 1975, ApJ, 201, 202
Fuller, G. M. 1982, ApJ, 252, 741
———. 1992, private communication
Fuller, G. M., Fowler, W. A., & Newman, M. J., 1980, ApJS, 42, 447
———. 1982a, ApJ, 252, 715
———. 1982b, ApJS, 48, 279
———. 1985, ApJ, 293, 1
Gaarde, C., Larson, J. S., & Rapaport, J. 1982, in Spin Excitations in Nuclei, ed. F. Petrovich et al. (New York: Plenum), 65
Goodman, C. D., & Bloom, S. D. 1982, in Spin Excitations in Nuclei, ed. F. Petrovich et al. (New York: Plenum), 143
Hansen, C. J. 1966, Ph.D. thesis, Yale Univ.
———. 1968, Ap&SS, 1, 499
Hartmann, D. H., Woosley, S. E., & El Eid, M. F. 1985, ApJ, 297, 837 (HWE)
Hillman, M., & Grover, J. R. 1969, Phys. Rev., 185, 1303
Holmes, J. A. 1976, Ph.D. thesis, California Inst. Tech.
Holmes, J. A., Woosley, S. E., Fowler, W. A., & Zimmerman, B. A. 1976, Atomic Data Nucl. Data, 18, 305
Kar, K., Sarkar, S., & Ray, A. 1991, Phys. Lett., 261B, 217
Koyama, S. I., Takahashi, K., & Yamada, M. 1970, Prog. Theor. Phys., 44, 663
Lanczos, C. 1964, Num. Anal. SIAM I, 86
Lederer, C. M., & Shirley, V. S., eds. 1978, Table of the Isotopes, 7th ed. (New York: Wiley)
Mazurek, T. J. 1973, Ph.D. thesis, Yeshiva Univ.
Mazurek, T. J., Truran, J. W., & Cameron, A. G. W. 1974, Ap&SS, 27, 261
Seeger, P. A., & Howard, W. M. 1975, Nucl. Phys., A238, 491
Takahara, M., Hino, M., Muto, K., Wolters, A. A., Glaudemans, P. W. M., & Sato, K. 1989, Nucl. Phys., A504, 167
Takahashi, K. 1971, Prog. Theor. Phys., 45, 1466
Takahashi, K., El Eid, M. F., & Hillebrandt, W. 1979, A&A, 67, 185
Takahashi, K., & Yamada, M. 1969, Prog. Theor. Phys., 41, 1470
Takahashi, K., Yamada, M., & Kondoh, T. 1973, Atomic Data Nucl. Data, 12, 101
Thielemann, F.-K., Arnould, M., & Truran, J. W. 1986, in Advances in Nuclear Astrophysics, ed. E. Vangioni-Flam et al. (Gif-sur-Yvette: Èditiones Frontiéres), 525
Vetterli, M. F., et al. 1989, Phys. Rev. C, 40, 559
von Groote, H., Hilf, E. R., & Takahashi, K. 1976, Atomic Data Nucl. Data, 17, 418
Wapstra, A. H., & Audi, G. 1985, Nucl. Phys. A, 432, 1
Weaver, T. A., & Woosley, S. E. 1980, Ann. NY Acad. Sci., 336, 335
———. 1992, Phys. Rep., submitted
Weaver, T. A., Woosley, S. E., & Fuller, G. M. 1985, in Numerical Astrophysics: In Honor of J. R. Wilson, ed. J Centrella, J. LeBlanc, & R. Bowers (Portola: Science Book International), 374
Weaver, T. A., Zimmerman, G. B., & Woosley, S. E. 1978, ApJ, 225, 1021
Woosley, S. E. 1985, in Proc. Accelerated Radioactive Beams Workshop, TRI-85-1, ed. L. Buchman & J. M. d'Auria (Vancouver: TRIUMF), 4
Woosley, S. E., Fowler, W. A., Holmes, J. A., & Zimmerman, B. A. 1975, Caltech Orange Aid Preprint, Vol. 422
Woosley, S. E., & Weaver, T. A. 1982, in Essays in Nuclear Astrophysics, ed. C. A. Barnes, D. D. Clayton, & D. N. Schramm (Cambridge: Cambridge Univ. Press), 377
———. 1988, Phys. Rep., 163, 79
Yokoi, K., & Yamada, M. 1976, Prog. Theor. Phys. Supp., 60, 161
Zaringhalam, A. 1983, Nucl. Phys., A404, 599